CENTRO DE INVESTIGACIONES
EN ÓPTICA, A.C.

Fringe projection technique: New methods for shape measurement

Thesis submitted in partial fulfillment of the requirements for the Ph.D degree in science (Optics)

by M. Sc. Analía Sicardi Segade

Advisor: Dr. Amalia Martínez García
Co-advisor: Dr. Julio César Estrada Rico

May 2015
León, Guanajuato, México

Comittee member
Dr. Amalia Martínez García

Comittee member
Dr. Abundio Dávila Álvarez

Comittee member
Dr. Cosme Furlong

"I am among those who think that science has great beauty. A scientist in his laboratory is not only a technician: he is also a child placed before natural phenomena which impress him like a fairy tale." Marie Curie

Contents

Acknowledgments

This thesis work would not have been possible without the financial support of the Mexican National Science and Technology Council (Consejo Nacional de Ciencia y Tecnología, CONACYT). It was an integral part of the project no. 180449, entitled: "Research and implementation of optical techniques in the evaluation of mechanical properties of materials and its topography". I wish to thank deeply the support of the CONACYT through scholarship grant no. 278883. This work took place in two laboratories: Optical Metrology IIIA and Digital Image Processing, Computer Vision and Artificial Intelligence, both at Centro de Investigaciones en Óptica (CIO). I thank for giving me the chance to work in these laboratories. I express my gratitude to Dr. Amalia Martínez García and Dr. Julio César Estrada Rico who supervised me through this thesis work, for their great availability for scientific discussions, and for the freedom they offered me during this work. I thank also Dr. Amalia for her understanding and her support during my stay in this research center. I thank B.S. Juan Rayas and M. Sc. Guillermo Garnica for all the support and help they gave me. Finally I thank all the members of my dissertation jury: Dr. Noé Alcalá Ochoa, Dr. Abundio Dávila Álvarez, Dr. Noel Ivan Toto Arellano and Dr. Cosme Furlong, for evaluating this work and for their valuable suggestions that will contribute to the improvement of its quality and my future work.

This thesis work is dedicated to my great family, who always supported me with their love and understanding.

Abstract

In this thesis, fringe projection technique is the base of the systems we built to measure objects topography and represents the core of this project. In the first part the fringes were generated by using a lateral cyclic shear interferometer (CSI). The topography obtained with this method is compared with the one obtained from a coordinate measuring machine (CMM). A study of the fringes visibility along the z axis is presented. The advantages and drawbacks of this profilometry system are discussed.

In the second part of this dissertation a basic fringe projection technique is adapted to deal with zero angle between projection and observation directions. The system presents sensitivity due to divergent projection which changes the fringes frequency in each one of the normal planes to z-axis. The accuracy of the new method proposed here is validated with real measurements obtained with a coordinate measuring machine (CMM) and compared with the standard fringe projection technique and a discussion of the advantages of the new method are reported.

Resumen

En esta tesis se presentan dos técnicas diferentes basadas en proyección de franjas para recuperar la topografía de objetos. En la primera parte, las franjas son generadas por medio de un interferómetro de desplazamiento lateral (CSI por sus siglas en inglés). La topografía obtenida por medio de este método es comparada con la topografía obtenida utilizando una máquina de medición de coordenadas (CMM por sus siglas en inglés). Se presenta un estudio de la visibilidad de las franjas a lo largo del eje z. También se discuten las ventajas y desventajas de este sistema de perfilometría.

En la segunda parte de esta tesis, la técnica de proyección de franjas es modificada para el caso en el que el ángulo entre las direcciones de proyeccion y observación es cero. El sistema presenta sensibilidad debido a la proyección de luz divergente, la cual cambia la frecuencia en cada uno de los planos normales al eje z. La exactitud de este nuevo método propuesto es validada con las mediciones reales obtenidas por medio de una máquina de medición de coordenadas y comparadas con la técnica tradicional de proyección de franjas y finalmente se reporta una discusión de las ventajas de este nuevo método.

1 Introduction

The need to measure different quantities has been very important for human beings throughout history. Since man lived in caverns, when he had the need to measure distances, he probably found that counting his steps could be a very simple and handy technique. Other human beings devised how to measure time using sundials. That need to measure this kind of parameters was so important as the most sophisticated measurements are important for us today. Thanks scientific knowledge and technology development in recent years, it is now possible to perform very complex measurements with a very good accuracy. With the advent of the laser in the 60s, great advances in the measurement technology were achieved, making big improvements in techniques that already existed in the field of optical metrology. These optical methods have the characteristics of being highly sensitive, very accurate, non contact, real time, programmable, whole field, among others. By having all these advantages, optical techniques can be a very good complement or exceed the capabilities of non-optical techniques, and they are sufficiently developed to be used in different industrial and scientific applications [1–3].

The motivation of this thesis focuses on non destructive techniques to obtain information from an object to be measured, in this case its topography. These techniques are an issue of great interest for a wide range of applications such as heritage protection, industrial, technical and medical applications [4–6].

In this thesis new contributions in the fringe projection technique are presented. In the first work, the projected fringes are generated by using a cyclic path interferometer of lateral shear which is stable against external vibrations. In the second part, a new fringe projection system is proposed, which presents the observation and projection positions on the optical axis (i. e. the angle between them is zero). The main advantage of this optical system is that the problems caused by the generation of shadows are removed. Other advantage of this method is that the shape recovery process is easier than the standard fringe projection method because the phase unwrapping algorithm is not necessary.

This thesis is organized as follows: Chapter 2 presents an overview of some optical measurement techniques and focuses on the fringe projection technique that is described in a separate section. In Chapter 3 an experimental setup of an interferometric fringes projection system is reported. The visibilty of the projected fringes is affected by the presence of speckle, and depends on the laser power used as of the distance between

object and projection system. The error is calculated in the topography measurement considering these parameters. In Chapter 4 a new method of the fringes projection is shown, where the angle between the projection axis and the camera axis is zero. In both works advantages and drawback of the systems are reported. In the Chapter 5 the phase recovery algorithms used in this thesis are presented. Finally conclusions and future work are shown in the Chapter 6.

2 Optical measurement methods

Optical measurement methods have the advantage of being highly sensitive, rapid, whole field and non-invasive, compared with other measurement techniques. Very recently, different optical methods have been developed to recover the topography at scales that range from the roughness of polished surfaces to natural scenery [1].

These methods are based in the modulation of the measurement by using any of the following parameters of the light: amplitude, phase, wavelength, frequency, polarization, and direction of light propagation. When the signal is demodulated we can obtain a particular point in space, a distance or an instant of time, both in discrete and continuous applications [1].

Some of the characteristics of the objects obtained by using optical metrology techniques are: refraction index, mechanical parameters or its topography. With these techniques the information from various objects or components can be obtained in a non-destructive and fast way. For this reason these techniques are widely used in industry, in automatic robotic vision, in medicine, in the protection of cultural heritage, security, navigation, object recognition, virtual reality, among many others [4, 5, 7].

Optical measurement techniques must be able to calculate the topography of an object (its shape and its physical dimensions) independently of the reflectivity of the object surface, its relief, the distance from the object to the sensor, and the light conditions [7].

In this chapter an overview of the techniques for optical shape measurement by means of CCD cameras is presented.

2.1 Characteristics of noncontact 3D shape measurements

Optical techniques for 3D shape measurement can be divided into three classes: *i)* Triangulation , *ii)* Time of flight measurement (TOF) and *iii)* Interferometry. Depending on the method used, the uncertainty changes with respect to the distance z from the sensor to the object. The range of measurement uncertainty, δz, can reach from a few nanometers to millimeters depending on the class to which the technique used belongs. In the Triangulation technique $\delta z \propto z^2$, in the Time of flight measurement $\delta z \propto cte$, and in Interferometry $\delta z \propto z^{-1}$ [7].

2.1.1 Triangulation

Techniques such as: *Focus techniques, Active triangulation with structured illumination, Passive triangulation techniques and Stereo Vision, Theodolite-measuring systems,* and *Shape-from-shading techniques* are within the triangulation class. All these techniques are based on determining a point of the measuring object using the parameters (sides and angles) of a known triangle formed with the optical measuring system and the object to be measured [7].

2.1.1.1 Focus techniques

Focus techniques have two important parameters to consider: 1) the diameter of the diffraction limited spot w, which is given by the following equation: [7]

$$w = 2.44\frac{\lambda f}{d} = 2f\sin\alpha\ , \tag{2.1}$$

and 2) the Rayleigh depth of focus Δz_R provided by the equation: [7]

$$\Delta z_R = \frac{\lambda}{\sin^2\alpha}\ , \tag{2.2}$$

where λ is the wavelength of light, $\sin\alpha$ is the numerical aperture, d is the diameter aperture of the optical system, and f is the focal length.

The group of focusing techniques includes techniques such as: *Confocal Microscopy, Controlled focusing,* and the *Defocusing Method.*

Next, a brief explanation of the *Confocal Microscopy* technique will be discussed.

Confocal microscopy: This technique is widely used in scientific research (biology and inspection of materials) as well as in the industrial sector. With this technique it is possible to increase the contrast and resolution of a given image. This can be achieved by placing a spatial pinhole in the confocal plane of a lens (objective lens), thereby eliminating the light coming out of focus. With this technique, it is possible to obtain the topography of different objects and structures by scanning in the x, y, and z axes. In Fig. 2.1 a diagram of the principle of confocal microscopy is shown [7, 8].

More information about the techniques *Controlled focusing* and *Defocusing Method* can be obtained in the following references [7–11].

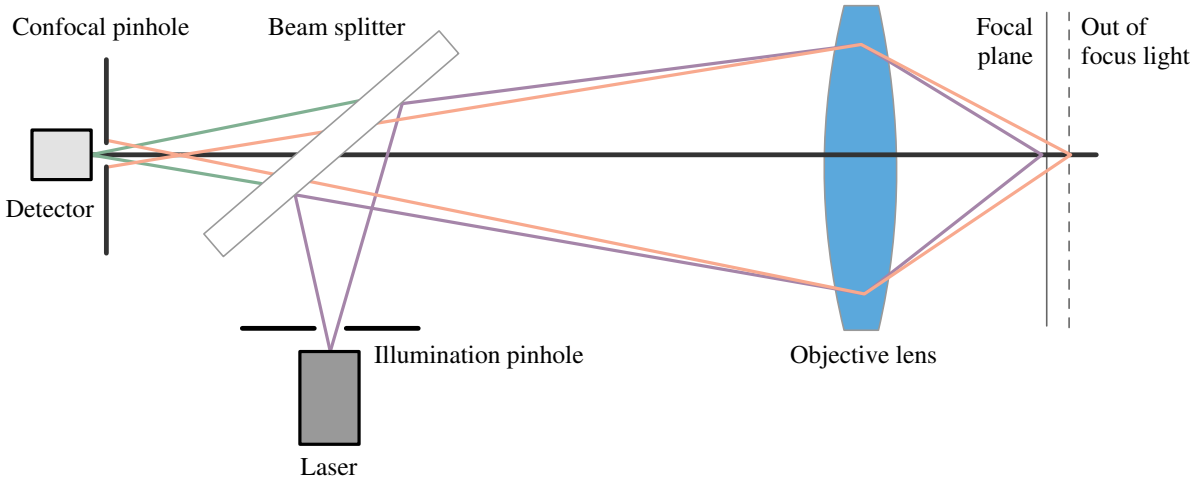

Figure 2.1: Principle of confocal microscopy.

2.1.1.2 Active triangulation

Active triangulation methods are based on the use of structured light for encoding. Structured light is the projection of a known pattern or set of known patterns of light on the scene where the object to be measured is placed. Each pixel in the projector has an associated code that is unique and different from the rest.

By projecting a known pattern on a scene, the pattern deforms. This deformation gives us information about the depth and shape of the object to be measured. With this technique different types of projections can be used; a point, a line or a grid [12].

-1D triangulation. Considering the point where the emission source projecting pattern is placed, the point where the detector is located in our system and a point of the object being illuminated by the projected pattern, the triangulation technique for measurement is obtained. The parameters of the system are obtained if we fix the base in the triangulation angle in the emission source and the angle in the detector is determined by the CCD camera. With these parameters established, the depth of the object can be determined. If we use laser light, the uncertainty in the measuring range Δz is given by : [7]

$$\Delta z = \frac{2\lambda}{\sin^2\theta}\ , \tag{2.3}$$

where $\sin\theta$ is the aperture of the optics detector.

-In the 2D triangulation technique, the laser beam can be expanded by using a cylindrical lens to be projected onto an object, or the object can be scanned with a device

that projects a light sheet. The projection of the lightsheet on the object generates a bright line that will scan the object in only one direction to obtain its topography. Fig. 2.2 shows a schematic of an instrument for 2D triangulation. If the plane of the detector has an axis in common with the plane where the optical system is located and the plane where the measuring object is found, the system will have the maximum depth resolution (*Scheimpflug condition*) [7, 13].

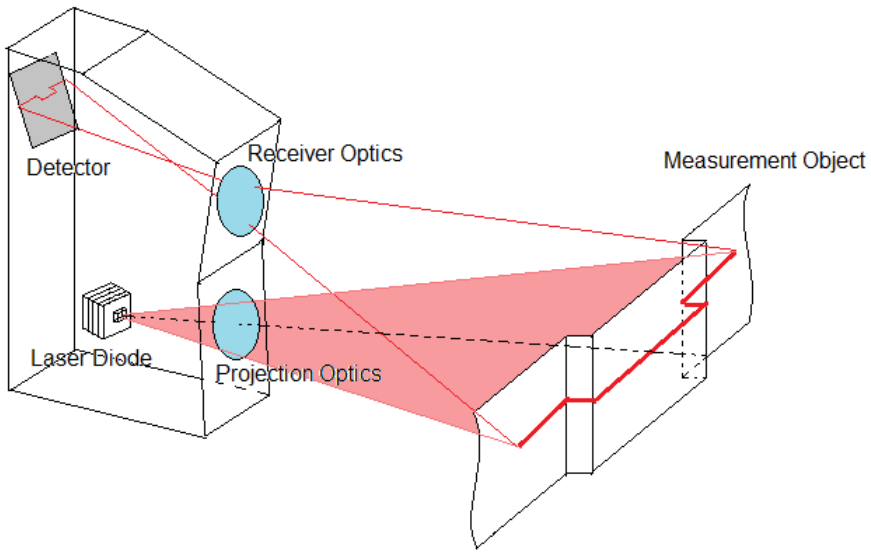

Figure 2.2: Lightsheet triangulation instrument.

-3D triangulation. The 3D triangulation technique does not need to scan the object to be measured because the entire object is illuminated in a single measurement. This technique uses structured light. The patterns that are generally used to project structured light are linear gratings, crossed lines and sinusoidal gratings. This method works well when the surface of the objects are smooth and non-specular. Due to the use of digital processing for object recovery, it is necessary that the values of neighboring pixels are known (to calculate the center point , the center of a line or the absolute phase of a sinusoidal gratings) and is therefore important that the object has lateral continuity of the surface [7, 14].

- For the Moiré technique, it is necessary to project a pattern on another reference pattern resulting in an overlapping patterns. These patterns are known as primary patterns and the pattern that is formed of overlapping primary patterns is called secondary pattern. The frequency of the secondary pattern, whose frequency is smaller than the primary patterns, is observed by a detector with the corresponding spatial

resolution. With this technique, the depth resolution can be improved by an order of magnitude compared to other fringe projection systems. [7, 15].

- Fringe projection technique. In this technique usually a multimedia projector that illuminates the object to be measured is used. The fringe pattern used in this method is usually sinusoidal. When the fringes pattern is projected on the object, the fringes are deformed and with this deformation the phase of the object can be obtained. With the phase information and the parameters of the arrangement (angle and sides of the triangle formed by the projector, the detector, and the plane where object to be measured is placed) the topography of the object is obtained. Phase recovery can be calculated by the Phase shifting technique or through Fourier transform technique, which are described in detail in Chapter 5 of this dissertation [7, 16].

2.1.1.3 Passive triangulation

The technique of passive triangulation includes all types of digital photogrammetry and stereovision. In this technique, the geometry of the arrangement is not considered, unlike the Active triangulation technique. In Passive triangulation, it is necessary to capture at least three images taken from different directions corresponding to the same point in order to determine the three-dimensional position of that point. If this technique is used for a static event, only a single camera that captures images of the event from different points of view is needed. However, if the technique is used in dynamic events, many cameras with their relative position known or having a method of autocalibration are necessary. With this technique, the topography is obtained by calculating the unknown parameters for the camera position at the same time with the points of the object [7].

2.1.1.4 Theodolites

Theodolites are optical measuring instruments used for measuring angles, both vertically and horizontally, and are widely used in surveying. They are also used in rocket launches and in the field of metrology to measure large-scale objects. Theodolites developed in recent years have a telescope placed between the horizontal and vertical axes (x and y respectively) and when the telescope points to an object it is possible to measure the angles of the x and y axes with precision of seconds of arc [17].

One of the great advantages of theodolites is that they have a relative error distance on the order of 5×10^{-6} m, and its main disadvantage is that measurement times are very long. To measure a 3D object using theodolites we need at least two of them, and the position of both need to be known. The coordinates of the angles of the x and y axes are then electronically calculated and the three-dimensional coordinates of the object to be measured are obtained [7].

2.1.1.5 Shape from shading

The *shape from shading (SFS)* is a technique that obtains the shape of the surface by taking a picture with a camera and analyze the brightness variations observed across the measurement surface. In order to calculate the 3D shape of the object to be measured it is necessary to know the position of the camera and light source that is in the setup. Techniques based on *shape from shading* can use many images with different illuminations or a sequence of images with moving light sources. This last technique is called photometric stereo [7, 18, 19].

2.1.2 Time of flight techniques

An easy way to determine the distance to any object or to determine the depth in the z axis is by using the principle of *time of flight (TOF)*. If we call τ the time it takes for a light signal from the moment it is sent by a sensor to return to the sensor, after being reflected by the object to be measured (as shown in the Fig. 2.3), we can calculate the traveled distance z by using the following equation [7]:

$$z = \frac{c\tau}{2} , \tag{2.4}$$

where c is the speed of light. This equation is valid for the *TOF* technique and the Interferometric technique for distance measurement. When the TOF technique is used, it is necessary to measure the group velocity when a modulated optical signal is used. This is done by correlating the signal with a reference signal such as a pulse modulation or continuous wave modulation. The disadvantage with all TOF techniques is that they use the speed of light as a parameter for calculation, so a very high temporal resolution is needed in order to measure distances [7].

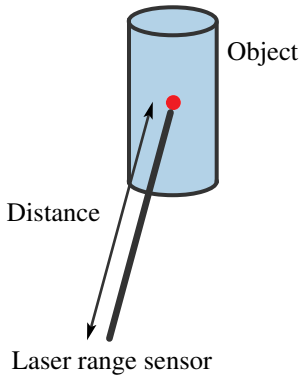

Figure 2.3: The principle of a time-of-flight sensor is shown in this figure.

2.1.2.1 Pulse modulation

One of the TOF techniques is the Pulse modulation technique. By using this technique the *flight of time* is measured directly using the correlation of a signal to start and to stop with a parallel running counter. The advantage of this technique is that it can distinguish many targets at once. However, their main disadvantages are: the delay that occurs because the system is sensitive to temperature, the nonlinearity of transients pulsed laser diodes and the bandwidth required for the system [7].

2.1.2.2 Continuous wave (CW) modulation

The principle of the continuous wave (CW) modulation technique can be explained as a radio wave interferometer with optical carrier modulation (RF Optical Interferometry (ORFI)). The echo of time of flight in a sine wave modulation can be calculated using a heterodyne mixing or a homodyne mixing. For higher resolution, to determine the time of flight of the dependent frequency shift or to detect pulse compression for the detection of many objects, the frequency modulated chirp modulation is used [7].

The TOF techniques are not widely used to measure topography (3D recovery) in industrial applications due to the high temporal resolution necessary, as stated at the beginning of this section [7, 20].

2.1.3 Optical interferometry

In the classical interferometry technique, a coherent light wavefront is divided in two wavefronts, one is the wavefront to be projected onto the object and the other is a reference wavefront. Both wavefronts will be superimposed on a detector, usually a CCD camera, what will produce an interferogram. Taking at least three interferograms with three phase shifts of the reference wavefront with respect to the wavefront of the object to be measured, it is possible to obtain the phase of the object being measured by using the technique of phase shifting (which is explained in Chapter 5). This technique can be applied to measurements of soft or polished surfaces. The disadvantage of this method is that you can not obtain the depth due to the ambiguity of the signal at $\lambda/2$ and its multiples. However with the use of homodyne and heterodyne interferometry it is possible to obtain a better resolution $\lambda/100$ and $\lambda/1000$, respectively. For good results with the interferometry technique, it is necessary to isolate the system from vibrations [7].

2.1.4 Multiwavelength interferometry

The technique of multiwavelength interferometry is widely used in industrial applications because it is theoretically possible to obtain (in ideal conditions) distance measurements up to 10 meters with a resolution on the order of nanometer. In this technique a beat frequency is generated by superimposing two frequencies with a very small separation, in the range of megahertz to gigahertz. The distance measurement can be taken without ambiguity in a range that is determined by the beat frequency [7].

2.1.5 Holographic interferometry

The digital holography technique records in a photosensitive device the information from a wavefront of coherent light such as a laser. The stored information is retrieved from the interference pattern of the wavefront reflected from an object before being deformed and after deformation [7].

Fig. 2.4 shows an example of the Holographic interferometry technique.

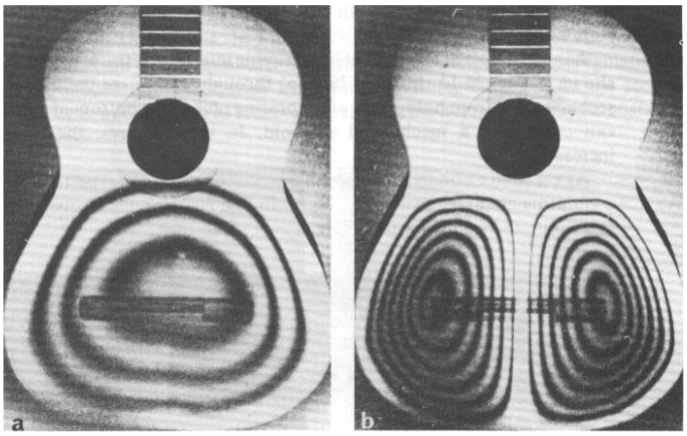

Figure 2.4: Example of Holographic interferometry. Vibrating guitar at: a) 185 Hz and b) 285 Hz. Images from Molin & Stetson, Institute of Optical Research, Stockholm, (1971) [21].

The digital holography technique also applies to the measurement of the topography or shape recovering of many objects with different shapes by its characteristic of being non-contact. A simple way to display the calculated information consists in obtaining contour maps, where the intersection of the measuring object with a group of equally spaced planes that are orthogonal to the line of sight can be observed [3].

2.1.6 Speckle interferometry

This technique was developed in the 70s. It was reported by Leendertz and Butters in 1970 and 1971 [22, 23], by A. Macouski, D. Ramsey, and L.F. Shaefer in 1971 and by O.Schwomma, with an Austrian Patent in 1972. Besides measuring deformation and stress, the speckle interferometry technique is also used for shape recovery. The setup scheme used for contouring can be seen in Fig. 2.5. It can be shown mathematically that the different speckle patterns are given by:

$$I_a - I_b = 4\sqrt{I_{ob} I_{ref}} \sin\left(\psi + {}^{\Delta\phi}/_{2}\right) \sin\left({}^{\Delta\phi}/_{2}\right) \ , \tag{2.5}$$

where I_a is the intensity of the speckle pattern when the object is not rotated, I_b is the intensity of the speckle pattern when the object is rotated an given angle, I_{ob} is the object beam intensity, and I_{ref} is the reference beam intensity. Furthermore, ψ is the phase difference of the wave coming from the object ϕ_{ob} and the wave coming from the reference ϕ_{ref}, and $\Delta\phi$ is the phase shift due to the rotation of the object.

The object height can be calculated based on the phase difference by using the following equation:

$$h(x, y) = \frac{\Delta\phi(x, y)\lambda}{4\pi w \sin\theta} \ , \tag{2.6}$$

where λ is the laser wavelength, w is the angle in radians that the object is rotated, and θ is the angle between the optical axis and the beam reflected by the mirror directed to the object. More information about the speckle interferometry technique can be found in the following references [1, 7, 24–32].

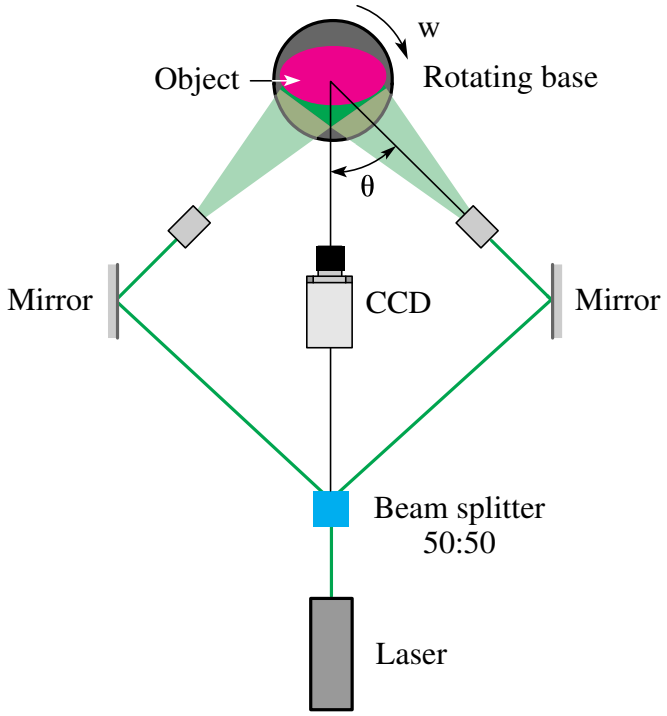

Figure 2.5: Schematic illustration of the setup for contouring by speckle interferometry.

2.1.7 White-light interferometry

The white light interferometry technique is used to calculate height measurements of three-dimensional surfaces ranging from tens of nanometers to a few centimeters.

By making interfere two waves using the superposition principle it is possible to obtain information about the resulting pattern as it is determined by the phase difference between the two waves (waves in phase form a constructive interference pattern and waves out of phase form a destructive interference pattern). Although the white light interferometry is not recent, by combining the known Interferometry techniques, electronics and programming, it is possible to obtain a measurement that is vary useful in many applications. Great advances in the field of white light interferometry and white light holography were reported by Yuri Denisyuk and Emmett Leith [33]. Fig. 2.6 shows an example of a white light Interferogram.

Because the white light has the feature that the achievable measuring uncertainty does not depend of the aperture of the illumination system and on the distance z, this method is used to measure with a great accuracy the depth of narrow wells boreholes. The arrangement is like a Michelson interferometer. At one end of the arm of the interferometer the sample is placed, on the opposite side there is a CCD camera, and

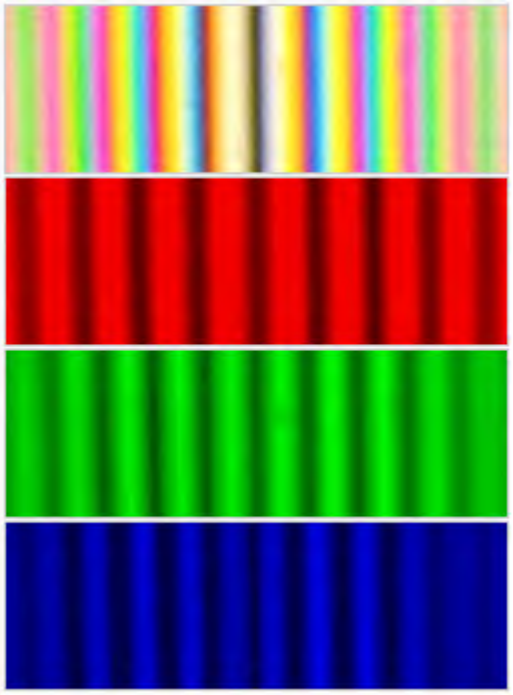

Figure 2.6: Above: white light interferogram. Below: red, green and blue channels of the white light interferogram shown above [33].

in the other end a movable mirror is placed. Fig. 2.7 shows a schematic layout of a white light interferometer [33].

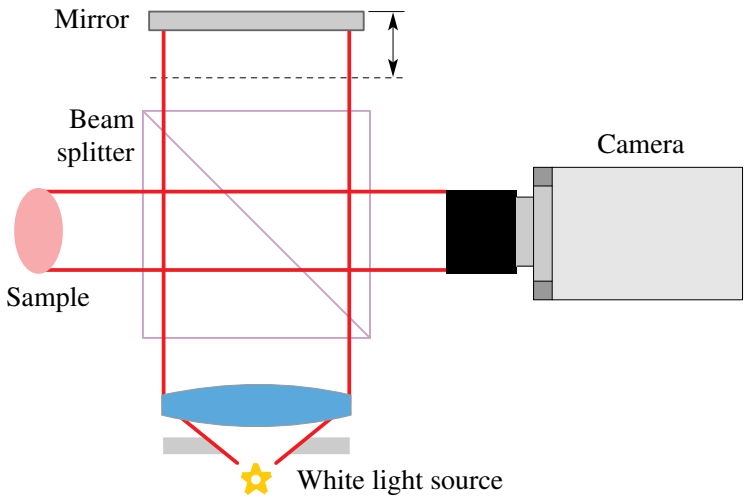

Figure 2.7: Schematic layout of a white light interferometer.

In this interferometer the white light interference occurs when the measuring beam and the reference beam paths are nearly equal. A very little change of the optical path of the reference beam introduced by moving the mirror generates an intensity curve in each pixel of the CCD camera. The width of this curve is the coherence length, which depends on the spectral width of the light source. Height differences in the measured object produces a phase pattern in the CCD sensor, which is combined with the light from the reference beam. In each pixel, interference occurs if the optical path difference between the two beams is less than half the coherence length of the light source. Each pixel gives us information about a different spatial position of the object's image to be measured. The maximum modulation of the interference signal of each pixel occurs when the optical path length of the light incident on the pixel is the same for the measuring beam and the reference beam. Finally, knowing where modulation is greatest for each pixel, it is possible to calculate the height of the surface of the object to be measured [33].

2.2 Fringe projection technique

One of the methods of active triangulation is the *Fringe Projection Technique,* which is considered one of the simplest to implement with good results in shape recovering. The research reported in this dissertation is based on this technique. This technique is used to measure topography and to make out of plane measurements. The fringe pattern to be projected may be formed by a projector, an interferometer or a grating structure.

The fringe projection method can easily measure the topography of an object at a certain angle between the observation and the projection point. Unlike the Interferometric technique, the fringe projection method allows object measurement with large height variation. In this technique, coherent and incoherent light can be used to project the fringes [34].

Next, the method will be described in detail. Fig. 2.8 shows a reference plane with fringes projected on it at an angle θ_1 with respect to the z axis with a period d. Due to the angle of projection the fringe period in the x axis is given by: [35]

$$d_x = \frac{d}{\cos\theta_1} \ . \tag{2.7}$$

If now the object S is placed on the reference plane, it can be seen that the fringe that was on point P_1 before placing the object is now placed on point P_2, where u is the

difference of displacement in the x axis between P_1 and P_2. This difference can be calculated as follows:

$$u = z(\tan\theta_1 + \tan\theta_2) \ , \tag{2.8}$$

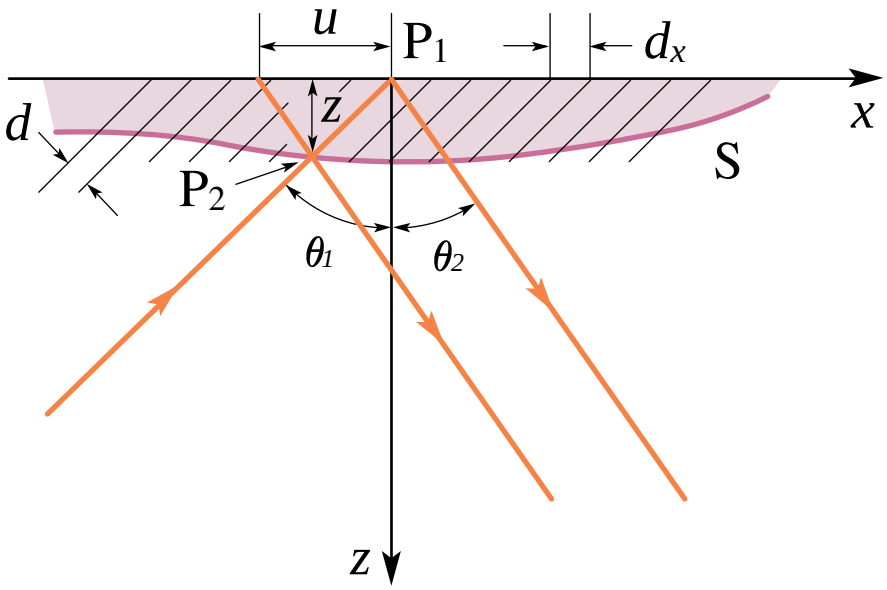

Figure 2.8: Fringe projection geometry. θ_1 represents the projection angle, and θ_2 the viewing angle.

where z is the height of P_2 with respect to the reference plane and θ_2 is the viewing angle. Moreover, u is equal to the number of fringes projected by the displacement along the x axis. The number of fringes N can be expressed as:

$$N = \frac{\Delta\phi}{2\pi} \ , \tag{2.9}$$

being $\Delta\phi$ the phase difference between the reference plane and the object. Then, u is given by

$$u = \frac{\Delta\phi}{2\pi} d_x = \frac{\Delta\phi}{2\pi} \frac{d}{\cos\theta_1} \ , \tag{2.10}$$

and z can be determined as:

$$z(x) = \frac{\frac{\Delta\phi}{2\pi} d_x}{\tan\theta_1 + \tan\theta_2} = \frac{\Delta\phi(x) d}{2\pi\left(\tan\theta_1 + \tan\theta_2\right)\cos\theta_1} \ , \tag{2.11}$$

corresponding to the S surface profile, assuming we are using collimated light [35].

If $\theta_2 = 0$ in Fig. 2.8, we obtain the arrangement most widely used in the Fringe projection technique. In Fig. 2.9, the standard setup for the fringe projection system is shown.

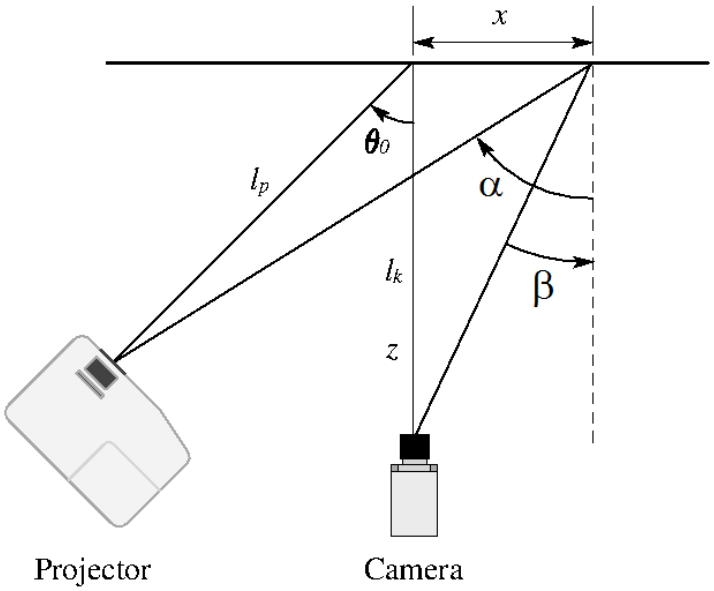

Figure 2.9: Fringe projection geometry.

In Fig. 2.9, θ_0 corresponds to θ_1 in 2.10, l_p is the projection distance, and l_k is the camera distance. If divergent illumination is used, it is possible to develop mathematical equations to get the following expression [35]:

$$z(x) = d_{x0} \cos\theta_0 \left[\sin\theta_0 + \frac{(l_k - l_p \cos\theta_0)\, x}{l_p l_k}\right]^{-1} \left[1 + \frac{x \sin\theta_0}{l_p}\right]^2 \frac{\Delta\phi(x)}{2\pi} \,, \tag{2.12}$$

where d_{x0} is the period of the fringe pattern at $x = 0$ [35]. If we call S (which can be called sensitivity vector) to the following expression that is part of 2.12

$$S(x) = \frac{d_{x0}}{2\pi} \cos\theta_0 \left[\sin\theta_0 + \frac{(l_k - l_p \cos\theta_0)\, x}{l_p l_k}\right]^{-1} \left[1 + \frac{x \sin\theta_0}{l_p}\right]^2 \,, \tag{2.13}$$

the height *z(x)* can be written as

$$z(x) = S(x)\Delta\phi(x) \,. \tag{2.14}$$

S is the sensitivity of the system, as it is shown in the reference [6].

The sensitivity of the system is a function of θ_0. When $\theta_0 = 90°$, the reference plane is parallel to the direction of the fringes, and perpendicular to the viewing angle. In this case, the system reaches its maximum sensitivity. However, when $\theta_0 = 90°$ shadows from the object might be projected on itself, and when the object is recovered, there could be areas that could not be recovered because of the shadows. On the other hand, when $\theta_0 = 0°$ the equation for shape recovery is indeterminate and results can not be obtained. The best way to get good results is when the angle θ_0 is not larger than the largest slope on the surface of the object to be measured.

In the following section, an experimental setup for an interferometric fringes projection system is reported. An error analysis in the shape recovery by using this setup and an analysis of the visibility of the projected fringes are presented.

3 Fringe projection technique by using a lateral cyclic shear interferometer

In this chapter the evaluation of the topography of an object with projected fringes generated with a lateral cyclic shear interferometer (CSI) is shown. The topography recovery obtained with this method is compared with the one obtained from a coordinate measuring machine (CMM). A study of how the fringes visibility along the z axis affects the retrieval is analysed. In the conclusion, the advantages and drawbacks of this profilometry system are discussed.

3.1 Introduction

In recent years, the use of the fringe projection technique for generating (3D) three-dimensional surface information has become one of the most active research areas in optical metrology [4]. The retrieval of the three-dimensional shape of an object is an issue of great interest for a wide range of applications such as heritage protection, industrial, technical and medical applications [5,6]. Coordinates measurement machines (CMMs) are well established and widely accepted in many applications. However, CMMs possess some limitations such as a high cost, a low measurement speed and the sparseness of the measurement points [6]. Common optical methods for surface profiling include the use of moiré and holographic interferometry, fringe projection and others [36]. Among them, the fringe projection method is considered the simplest one because optical fringes can be generated and projected easily with a Michelson interferometer [37]. But the use of this type of interferometer requires stringent vibration-free testing conditions, thereby confining its applications to the laboratory environment [36]. In this thesis we present a lateral cyclic shear interferometer (CSI) to generate projected fringes. This has the advantage of generating stable fringes with little vibration isolation. We also evaluate the influence of the visibility of the fringes and how this affect the recovery of the topography by analyzing the visibility as a function of the distance between the object and the projection system, and as a function of the laser power too, and we compare the retrieval of the test object for some values of the z axis, with the retrieval obtained from a CMM. Finally, we calculate the experimental resolution of the optical system as a function of the distance.

3.2 Common-Path Interferometer

In many interferometers the reference beam and the sample beam follow separate paths that can be affected differently by mechanical vibrations. This can produce an instability in the projected fringe pattern, and in these conditions it is impossible to obtain good measurements. This does not happen in common path interferometers, where the reference beam and the sample beam travel the same path. If there are any vibrations, both beams are affected exactly in the same way [38–45].

3.3 Experimental setup

In Fig. 3.1, the CSI used as a fringe projection system is shown, where the shear is generated by moving the mirror M by a small distance Δs. A Verdi laser emitting at 532 nm (2 W maximum output power), was expanded and spatially filtered using a 60× microscope objective lens and a 20 μm diameter pinhole. Divergent illumination and output laser powers of 20, 40, 60 and 80 mW were used to find the best visibility.

The fringe pattern is generated as follows. Light passes through the spatial filter and then through the first linear polarizing filter placed at 45 degrees with respect to the laser's polarized light transmission axis. After that, the light beam passes through the polarized beam-splitter (PBS), where it is divided into two beams. The beam-splitter is designed to transmit one of the beams with a horizontal polarization, while the other one is reflected with a vertical polarization. Both beams are reflected in the two mirrors M and M', that are placed initially at a distance d from the beam-splitter. The vertical polarized beam arrives to mirror M' and is reflected to mirror M, where it is reflected back to the PBS. The horizontal polarized beam arrives to mirror M where it is reflected to mirror M' before arriving to the PBS. When both beams get outside the polarized beam-splitter, one beam polarization is perpendicular to the other one and a polarizing linear filter P_0 is needed in order to make that both beams components interfere [46, 47]. The fringe pattern can then be seen in a reference plane, and the fringes pitch can be adjusted by moving the mirror M.

The use of the polarizing filters and the PBS is to obtain the best visibility. The fringes pattern can also be obtained by using a non-polarizing 50:50 beam-splitter and without the polarizing filters, but in that case the visibility of the fringe-pattern would be smaller because the transmission and reflection beams are not exactly 50:50 in practice, that is, there is a little difference between the two beams. By using the polarizing filter and the PBS we can obtain the best contrast rotating the polarizing filter P_0 to find the best visibility.

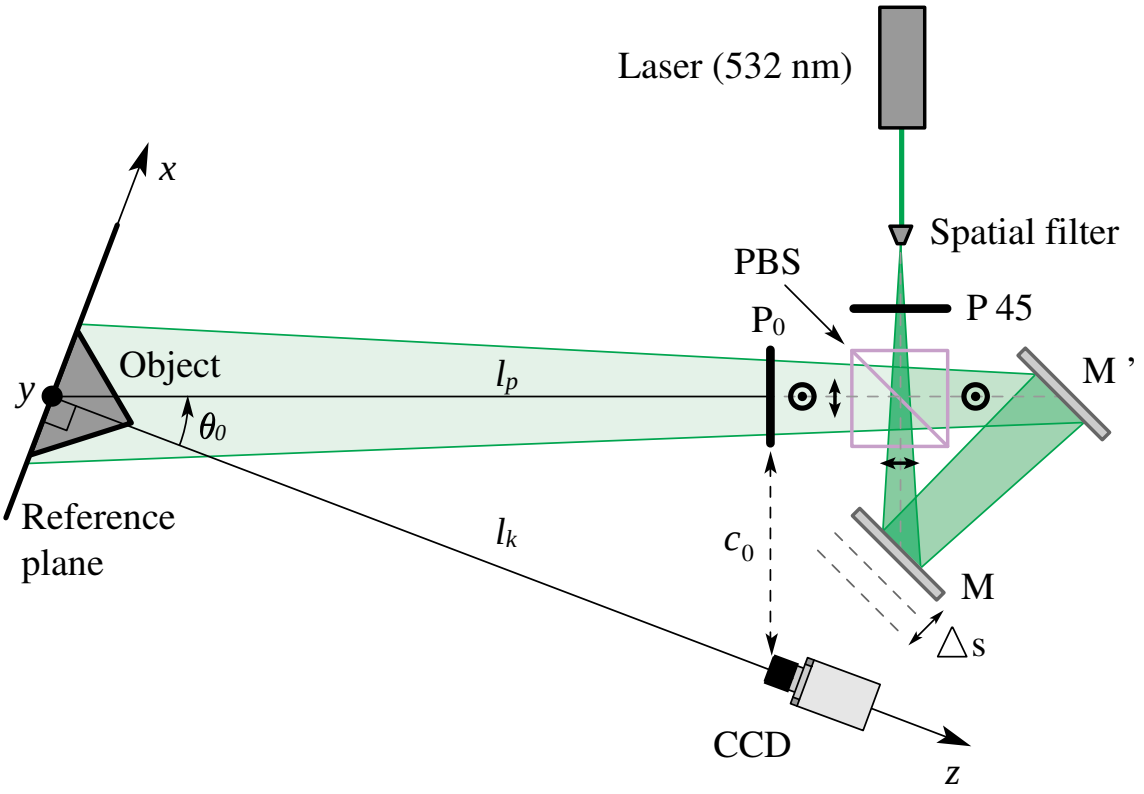

Figure 3.1: Fringe projection system using a CSI. M and M': Mirrors, PBS: Polarized 50:50 Beam-Splitter, P_{45}: linear polarizing filter placed at 45 degrees with respect to the laser polarized light, P_0 : linear polarizing filter used to make both beams components interfere, l_p: distance between the array and the reference plane, l_k: distance between the camera CCD and the reference plane and is the angle between l_p and l_k.

The CSI is placed in a standard fringe projection setup replacing the multimedia projector as shown in Fig. 3.1.

In the case of parallel illumination and parallel observation, the equation to retrieve the three-dimensional shape is [35]

$$z = \frac{\Delta\phi(x,y)p}{2\pi tan\theta_0}\,, \tag{3.1}$$

where p is the fringes pitch and $\Delta\phi(x,y)$ is the phase difference between the test object and the reference plane. With the use of non-collimated illumination the topography

can be obtained by the following two equations [6, 35]

$$z = \Delta\phi(x, y)S(x) \ , \tag{3.2}$$

where S [mm/rad] is the sensitivity of the system and it depends on the set-up geometry [6, 35], and

$$S = \frac{p_{xo}}{2\pi} cos\theta_0 \left[sin\theta_0 + \frac{(l_k - l_p)cos\theta_0 x}{l_p l_k} \right]^{-1} \left[1 + \frac{x sin\theta_0}{l_p} \right]^2 \ , \tag{3.3}$$

where p_{xo} is the pitch of the fringe at $x = 0$, θ_0 is the angle between the projection and the observation directions, l_p is the distance between the polarizer P_0 of the CSI and the reference plane for $x = 0$, and l_k is the distance between the CCD and the reference plane at $x = 0$ [6].

3.4 Results and discussions

In this section we present some experimental results of the fringe projection profilometry system used to retrieve the three-dimensional shape of an object. The test object is a pyramid with a base of 89 *mm* x 89 *mm* and a height of 48 mm. Fig. 3.2 shows the experimental optical system used to project fringes over the test object. Fig. 3.3 shows the pyramid with the projected fringes, Fig. 3.4a shows the topography obtained by measuring some points with a CMM and Fig. 3.4b shows the topography obtained by using the projected fringes technique. To retrieve the object with the CMM method, 41 surface points were measured. After that, interpolation and extrapolation were necessary to complete the surface and to recover the topography of the pyramid.

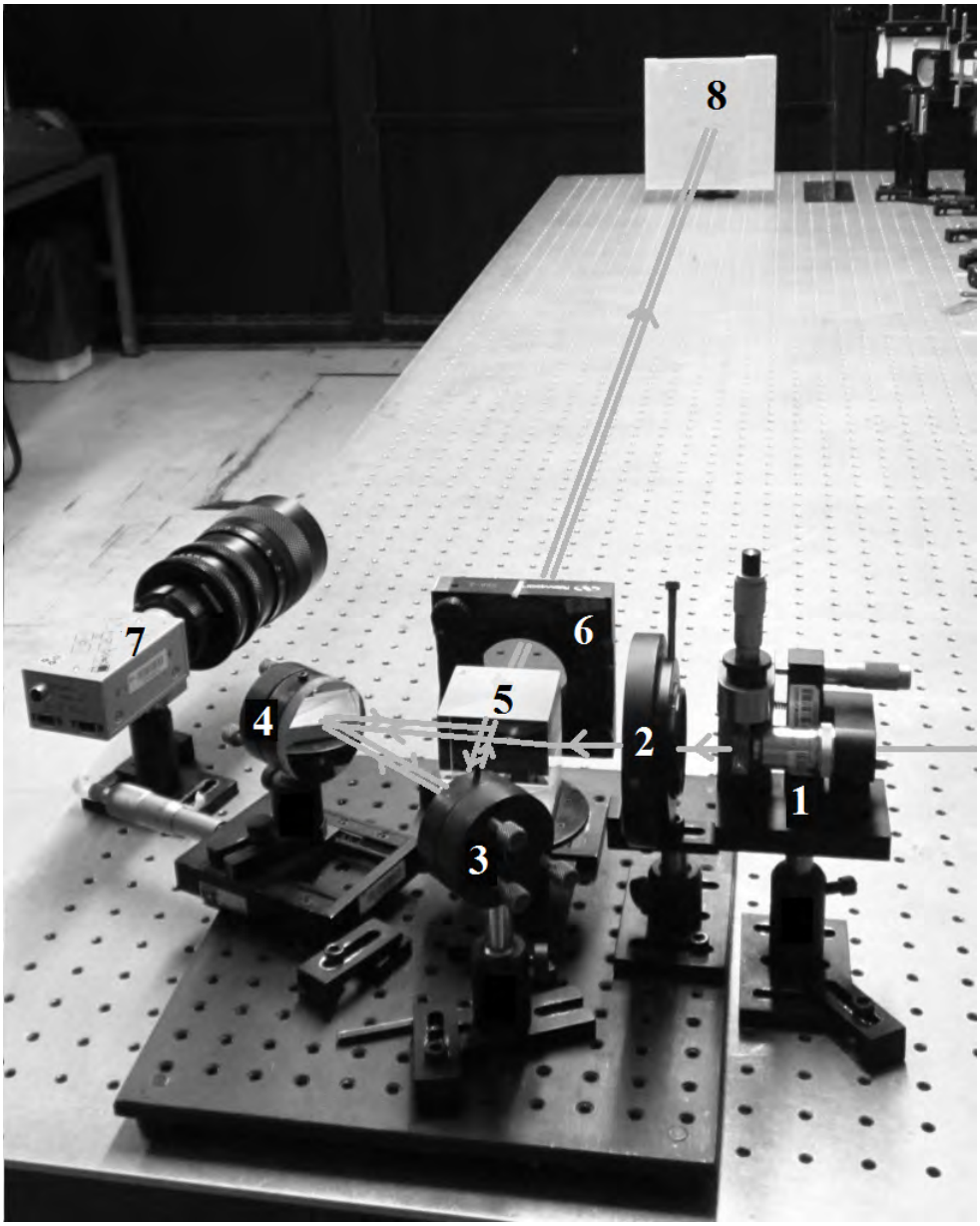

Figure 3.2: Experimental array. 1. Spatial filter, 2. Polarizer placed at 45 degrees with respect to the laser's polarized light transmission axis, 3. Mirror, 4. Mobile mirror, 5. PBS: Polarized Beam-Splitter, 6. Linear polarizing filter used to make both beams components interfere, 7. CCD, 8. Reference plane. The arrows show the beam path.

The Fourier-transform technique was used to recover the wrapped phase of the projected fringe pattern [14]. To unwrap the phase of the object, a noise robust algorithm was programmed [48]. The experimental results obtained with the projected fringes

technique by using Eq. 3.2 in the case of non-collimated illumination, show a maximum error of 4.5 % in the topography measurement, taking as a reference the measurement obtained with the CMM. In this case, the distance between the reference plane and CCD was l_k= 160 cm and the distance between the projection head and the reference plane was l_p = 158.9 cm. The laser output power was 60 mW.

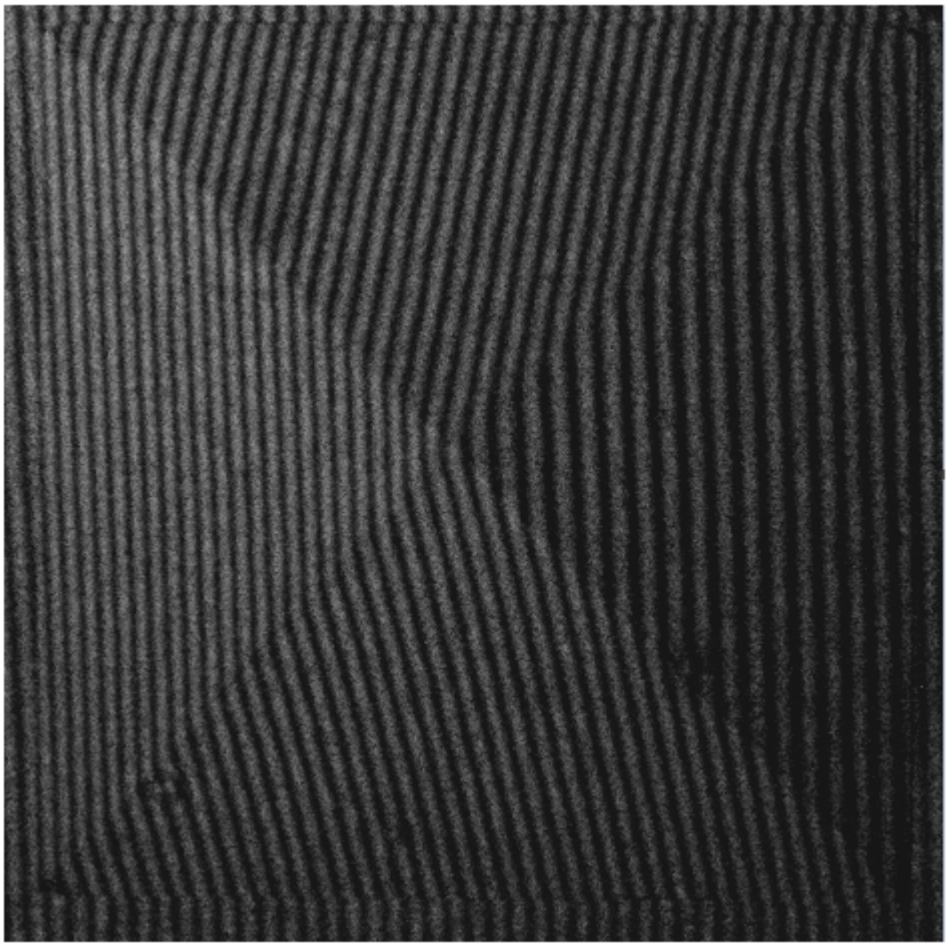

Figure 3.3: Fringes projected on a white pyramid.

Fig. 3.5 shows topography profiles by using equations 3.1 and 3.2, which are compared with profile obtained from the CMM in a) $y = 0$ and b) $x = 0$. It can be observed that the topography evaluated by using Eq. 3.2, which takes into account the divergent illumination, is close to the topography obtained by the CMM.

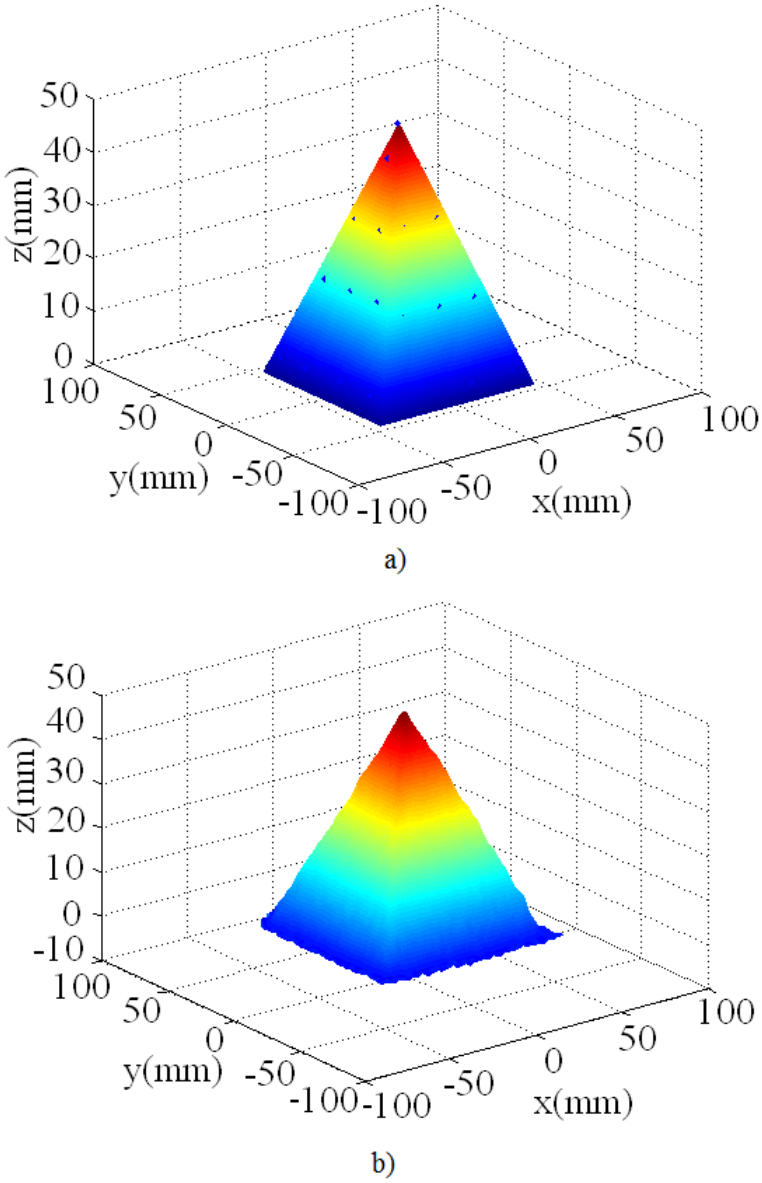

Figure 3.4: Topography of the pyramid obtained by: a) measurements from the CMM, and b) our fringe-projection technique.

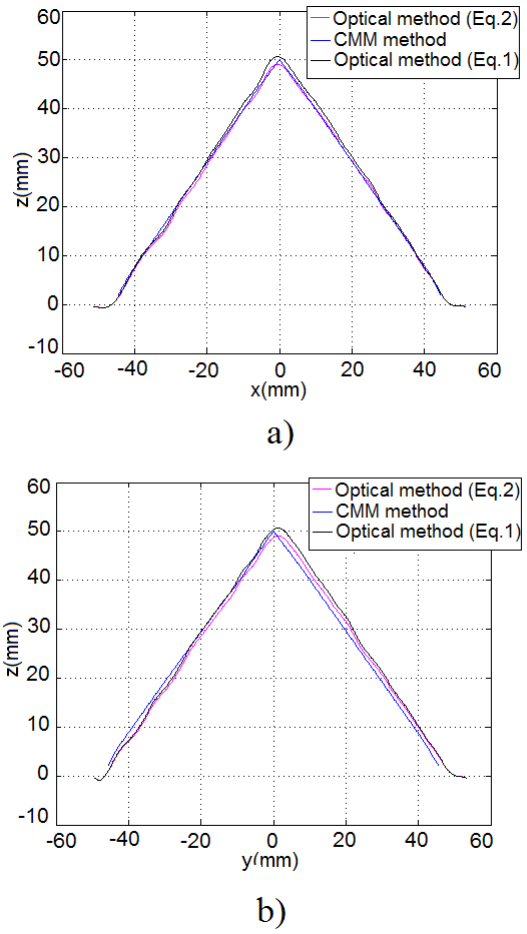

Figure 3.5: Measurements obtained from the CMM (dashed-point line) and the optical method by using Eq. 3.1 considering collimated illumination (continuous line) and Eq. 3.2, non-collimated illumination (dashed line), in: a) $y = 0$, and b) $x = 0$.

3.5 Analysis of the projected fringes visibility generated by a CSI

The fringe pattern is recorded by a CCD at different positions along the optical axis. The distance between the reference plane center and the CCD is from 60 cm to 200 cm. The fringe pattern is recorded each 10 cm. The output power of the laser used was 20 mW, 40 mW, 60 mW and 80 mW, at every position of the CCD. Fig. 3.6 shows the fringes visibility as a function of the distance between the reference plane center and the CCD for the different powers employed. As can be seen from Fig. 3.6, the visibility obtained at the CCD positions between 60 and 90 cm is higher for the lowest power

used, that is, 20 mW. This is due to the saturation of the CCD for powers larger than 20 mW. However, 20 mW is not enough power for distances greater than 90 cm and the fringes visibility decrease. For distances longer than 90 cm higher powers are needed in order to increase the fringes visibility. In the CCD position corresponding to 200 cm, the best visibility is obtained for a power of 80 mW (up to 60%). Next, we fixed the distance at 200 cm and changed the laser power in order to find the power that increases the fringes visibility. Fig. 3.7 shows that a visibility of 89% is reached for a power of 120 mW. For higher values, the visibility decreases due to the saturation of the CCD. The visibility (or contrast) was calculated by using the following equation [49]

$$V = \frac{I_{max} - I_{min}}{I_{max} + I_{min}} \, . \tag{3.4}$$

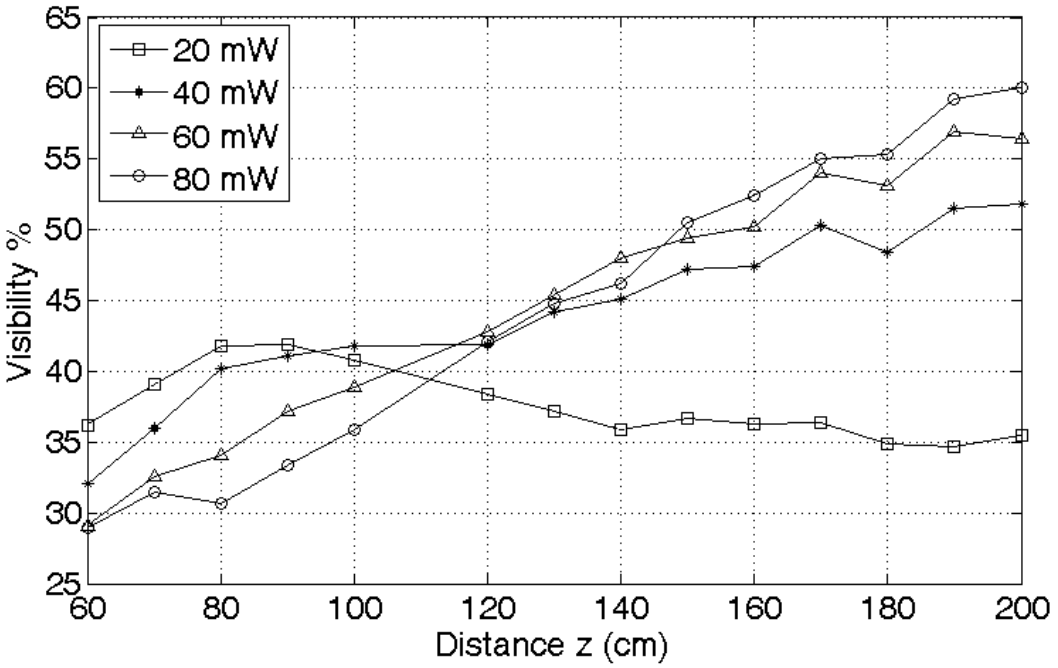

Figure 3.6: Visibility as a function of distance for different laser powers.

The visibility was calculated by considering the average intensity of each column of the fringe pattern and then calculating the maximum and the minimum intensity of the resulting array. Fig. 3.8 shows a fringe pattern and its intensity profile used to determine the visibility.

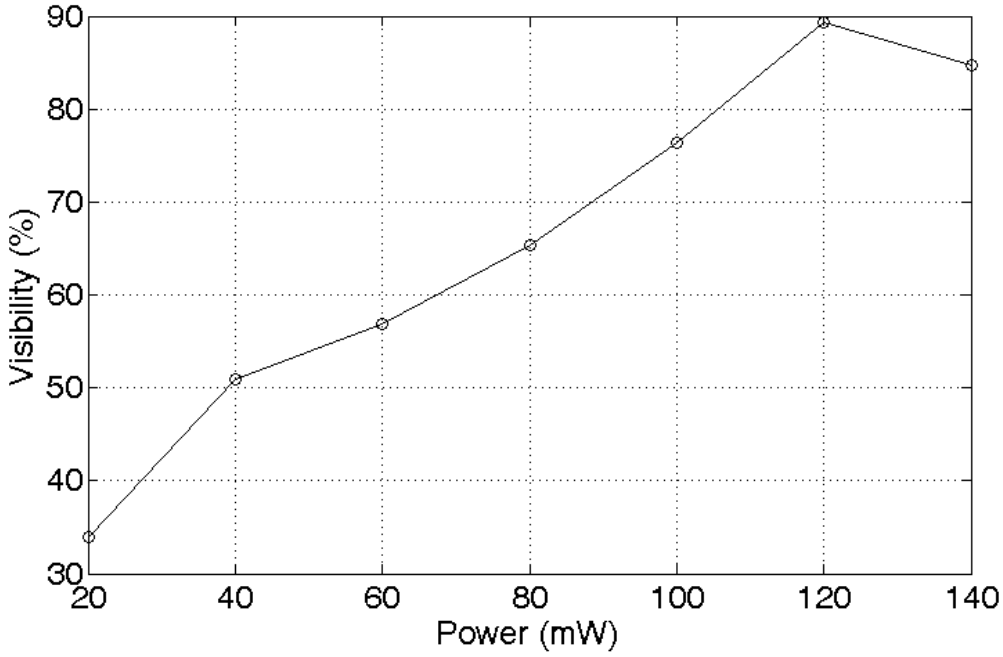

Figure 3.7: Visibility versus laser's power at z = 200 cm.

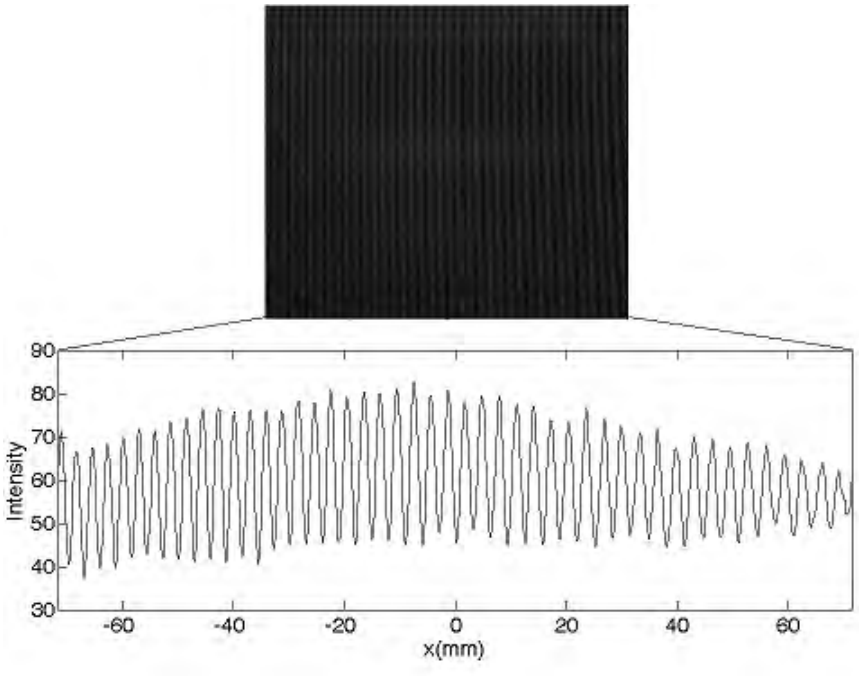

Figure 3.8: Fringe pattern and its intensity profile.

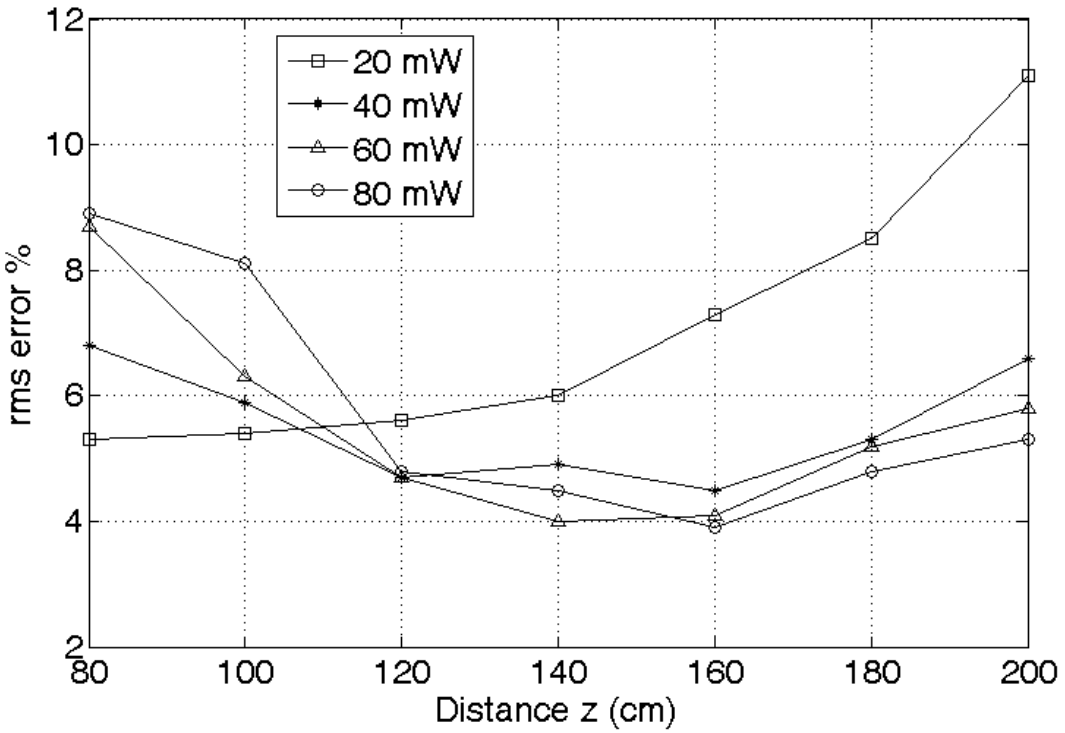

Figure 3.9: Curves of topography error versus distance for different powers.

Fig. 3.9 shows the root-mean-square error (*rms*) associated to the topography measurement versus CCD position and for different laser powers. It is observed that the fringes visibility affects the measurement of the topography. We found a maximum error in the topography measurement of 9 % for a power of 80 mW with the CCD placed at 80 cm to the reference plane. In this same CCD position, an error of 5.4% is obtained for a power of 20 mW. At 200 cm, the error increases to 11% for a power of 20 mW while the error decreases to 5.3% when the power used is 80 mW. The error was calculated based on the measurements obtained from the CMM.

Finally, we calculated the experimental resolution of the optical system i. e. the minimum z that can be measured. To calculate the minimum z, Eq. 3.1 was used considering that the fringe moves one period when the object is placed instead of the reference plane. Assuming that, the relation $^{\Delta\phi}/_{2\pi} = N =$ order of the fringe $= 1$ holds. As a consequence, Eq. 3.1 can be written as [50]

$$\Delta z = \frac{p}{tan\theta_0} \ . \tag{3.5}$$

Now, to calculate the z_{min}, we consider the fringe moving only one pixel in one period,

that is

$$z_{min} = \frac{\Delta z}{number\,of\,pixel\,per\,period} = \frac{\frac{p}{tan\theta_0}}{number\,of\,pixel\,per\,period} \,. \tag{3.6}$$

Fig. 3.10 shows the experimental resolution obtained as a function of the distance. It can be seen that the resolution improves when the distance between the optical system and the reference plane is decreased.

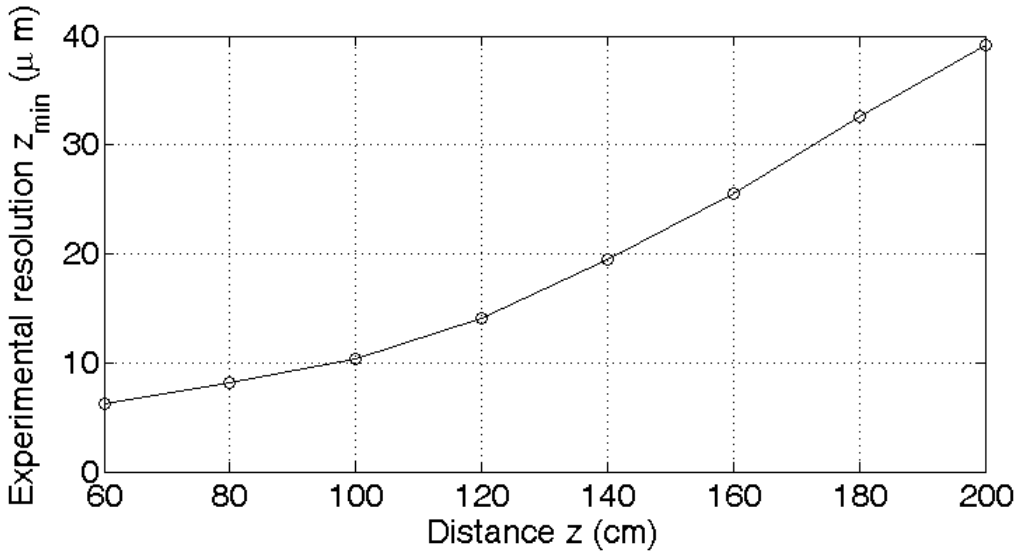

Figure 3.10: Experimental resolution of the system versus distance.

3.6 Conclusions

In this work we proposed a linear cyclic shear interferometer to generate projected fringes. Being a cyclic path this interferometer is quite stable, therefore one of the advantages of this method is its capability to generate stable fringes in poor vibration isolation conditions.

The fringe-pattern projected by an interferometric system has the advantage of being absolutely sinusoidal, unlike the one generated with a multimedia projector. Moreover, with a fringe projection interferometer, synchronization with a CCD camera is not necessary.

By using this method, the pitch of the fringes can be varied by changing Δs, which means that both large and small objects can be measured.

One of the disadvantages of this optical system is that the size of the object to be measured is limited by the size of the beam-splitter, which imposes a limit to the expansion of the beam to cover a large object placed at a short distance.

In this work, we also presented an analysis of how the visibility of projected fringes affects the evaluation of the topography of an object by using fringes generated by interferometry.

4 On axis fringe projection

The traditional fringe projection technique requires a non-zero angle between projection and observation directions to have sensitivity in the z direction. In this chapter, a new method for shape measurement using fringe projection is presented. In our case, the angle between projection and observation directions is zero, but the system presents sensitivity due to divergent projection which changes the fringes frequency in each one of the normal planes to z-axis. The accuracy of the new method proposed here is validated with real measurements obtained with a coordinate measuring machine (CMM) and compared with the standard fringe projection technique. Finally, we discuss the advantages of the new method.

4.1 Introduction

The use of the fringe projection technique for generating three-dimensional (3D) surface information has become one of the most active research areas in optical metrology during recent years [4,35]. The retrieval of the three-dimensional shape of an object is an issue of great interest for a wide range of applications such as heritage protection and industrial, technical and medical applications [5]. Standard fringe projection systems use an off-axis setup for doing profilometry [4,35], but due to this configuration objects may present shadow areas where no fringe patterns are formed and, as a result, it would be impossible to obtain the elevation measure [51]. Many contributions to resolve the shadows problems have been reported. A.F.M. Hani et al. [51] proposed an image processing method using wavelet analysis for shadows detection. Bringier, et al. [52] proposed a photometric stereo method to detect shadow and specularity. Skydan et al. [53] proposed a method for shadows detection using a camera, two projectors and colored structured light. M. Sasso, et al, J. Harizanova, et al and Y.Hao et al [54–56] have proposed methods based on the use of multiple projectors. All these techniques are more complex because they use more than one projector or need additional image data processing to solve the problem.

Standard fringe projection method use a setup out of axis and the equation used to recover the shape is:

$$z(x,y) = \frac{\phi(x,y)}{2\pi} \frac{p}{tan\alpha + tan\beta} \ , \tag{4.1}$$

where $\phi(x, y)$ is the phase of the object, p is the pitch of the fringe pattern, α is the angle between the optical axis and the observer, and β is the angle between the optical axis and the projection direction like is showed in Fig. 4.1 [35]. It is easy to see that there is an indetermination in the equation when the system is on axis (i.e., $\alpha = 0$ and $\beta = 0$). However, if we could have an on axis fringe projection system, the problem with the shadows could be significantly reduced. In the following section, we show how to recover the object profile using a projected fringe pattern by using an on axis projection system. A pin-hole camera model is used to obtain the fringe pattern modulation by means of divergent rays. A theoretical model will be shown and it will be supported by experimental results. Discussions and conclusions will be given at the end of this chapter.

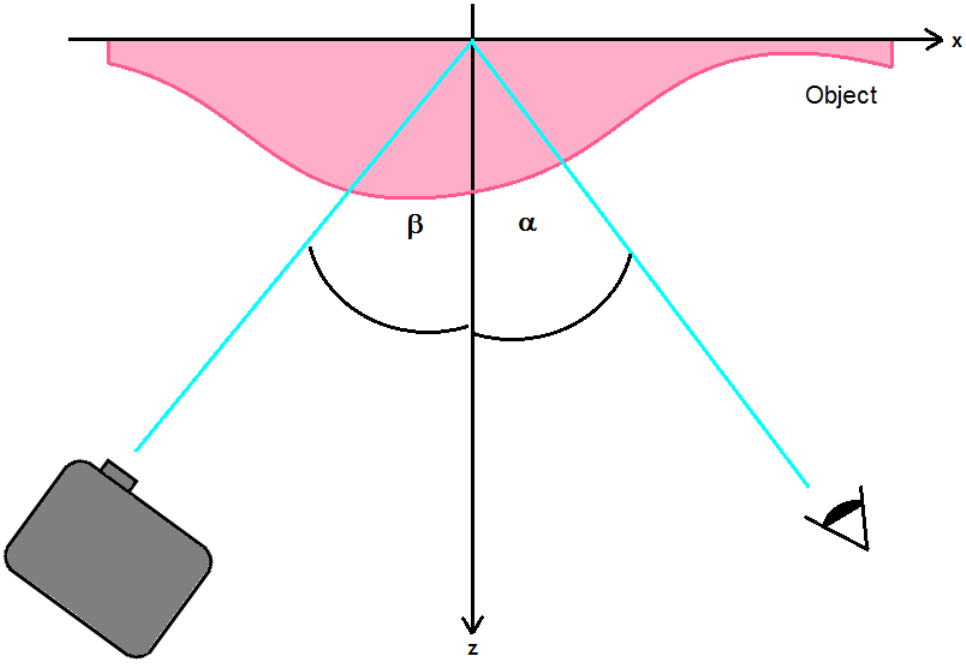

Figure 4.1: Fringe projection setup out of axis.

4.2 On axis fringe pattern model

Let's consider a 3D orthogonal coordinate system with a camera placed at the origin O and a pinhole camera model, for simplication purposes [57]. The z axis is pointing in the viewing direction of the camera and is referred to as the optical axis. The

reference plane S_0 with fringes projected on it is placed at a distance L_0 from the origin. The y axis is perpendicular to Fig. 4.2. Without taking into account the background illumination, the equation for the fringe pattern on the reference plane S_0 can be written as:

$$I_0(x) = cos(\omega_0 x) \ , \tag{4.2}$$

where $w_0 = 2f_0$ and f_0 is the frequency of the fringes pattern projected at the reference plane. Only the light ray coming from a point P positioned at the plane S_0 with coordinates (L_0,p) which passes through the hole at the origin of the camera coordinate system meets the image plane at point P_i [57]. If we move S_0 a distance z from the image plane, perpendicularly to the optical axis, the plane would be located at position S_1, and the point P would be shifted to position P' with coordenates (z, p). Now, the light ray passing through the center of the system O towards point P' intersects the plane S_0 in P'' with coordinates $(L_0, p + \Delta p)$ corresponding to point P_i'' at the image plane. The fringe pattern image I_1 can be written as:

$$I_0(x) = cos(\omega_1 x) \ , \tag{4.3}$$

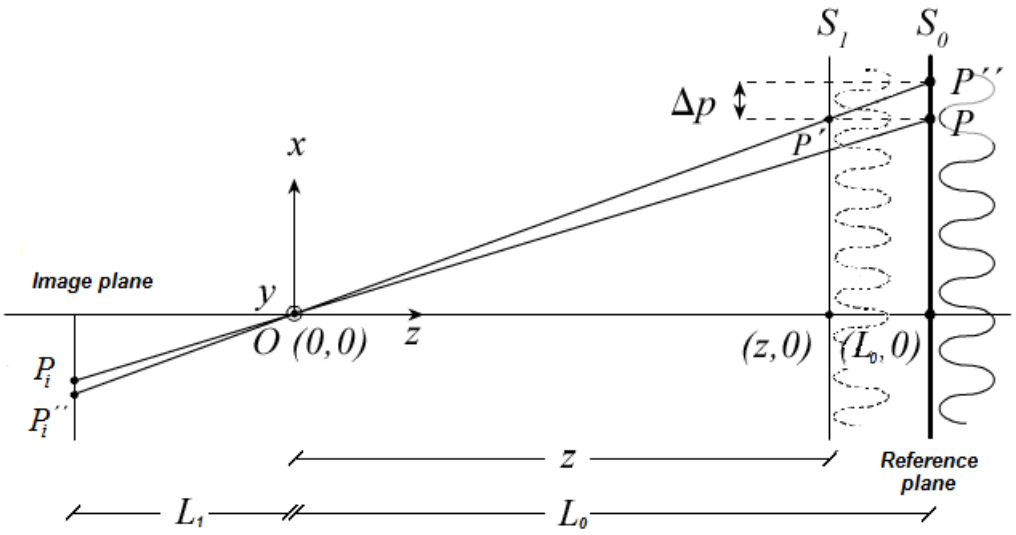

Figure 4.2: Geometry of the model as seen from the y axis.

where $w_1 \neq w_0$ due to the fact that we are using divergent illumination. Now, we can

obtain z by calculating the intersection of the ray $\overline{OP''}$ with the straight line $\overline{P'P}$. That is:

$$\begin{cases} \overline{OP''}: & x = \frac{p+\Delta p}{L_0} z \\ \overline{PP'}: & x = p \end{cases} , \tag{4.4}$$

and solving for z, from the system equations we obtain:

$$z = \frac{pL_0}{p + \Delta p} , \tag{4.5}$$

where all the parameters are known, except Δp. By using Eqs. 4.2 and 4.3, Δp can be calculated. In order to do that, Eq. 4.3 can be rewritten as:

$$I_1(x) = cos(\omega_1 x) = cos(\omega_0 x + \Delta\phi(x)) , \tag{4.6}$$

where $\Delta\phi$(x) is a shift in the x axis. On the other hand, if we shift the point x a distance Δp we have:

$$I_0(x + \triangle p) = cos(\omega_0 x + \omega_0 \Delta p) = cos(\omega_0 x + \Delta\phi(x)) , \tag{4.7}$$

and then, the following equalty holds:

$$\omega_0 x + \omega_0 \Delta p = \omega_0 x + \Delta\phi(x) . \tag{4.8}$$

Solving for Δp we obtain:

$$\Delta p = \frac{\Delta\phi(x)}{2\pi f_0} . \tag{4.9}$$

Finally, substituting Eq. 4.9 into Eq. 4.5 we find the equation for z in terms of known parameters:

$$z(x) = \frac{pL_0}{p + \frac{\Delta\phi(x)}{2\pi f_0}} , \tag{4.10}$$

But, as we are interested in the height differences (*h(x)*) measured from the reference plane, we get for a 2D system:

$$h(x) = L_0 - z(x) = L_0 - \frac{pL_0}{p + \frac{\Delta\phi(x)}{2\pi f_0}} \ , \tag{4.11}$$

Finally, the system equations for all the rows, *h(x, y)*, can be expressed as:

$$h(x,y) = L_0 - z(x) = L_0 - \frac{xL_0}{x + \frac{\Delta\phi(x,y)}{2\pi f_0}} \ . \tag{4.12}$$

Eq. 4.12 allows to recover the 3D object profile for all *x, y*, except for points in the vertical line $x = 0$, because when $x = 0$, $\Delta\phi(x, y) = 0$ and there is an indetermination in the equation right second term.

The latter can be claried with the help of Fig. 4.3a that shows the reference plane perpendicular to the optical axis in 3D with a fringe pattern projected on it. If we place a new plane a distance *h(x, y)* in front of the reference plane, we could see that the fringes that are in both sides of this plane would move laterally, but the one that is in the optical axis wouldn't. This effect is shown in Fig. 4.3b.

This corresponds only to the fringe that is at the optical axis, and therefore, $\Delta\phi(x, y) = 0$ when $x = 0$ and we can not recover *h(x, y)* at the optical axis. However, this can be solved by interpolating *h(x, y)* for $x = 0$ once we have estimated their neighborhood, or the object can be placed in a position where it does not cross the optical axis.

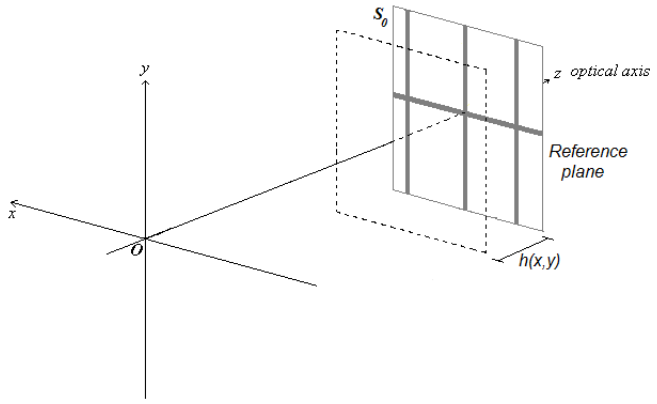

a)

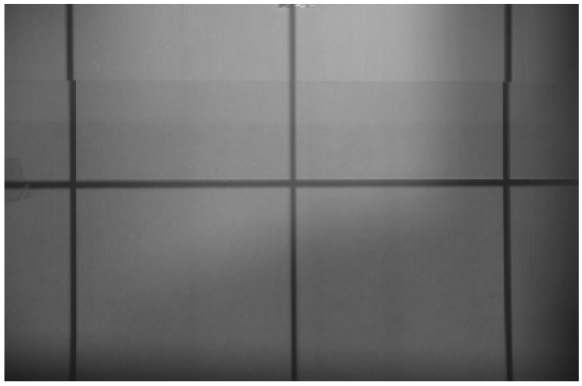

b)

Figure 4.3: a) Diagram of the reference plane aligned with the optical axis in 3D, b) image captured with the camera showing the fringe shift when an aditional plane of smaller height is placed in front of the reference plane.

4.3 Experiment and results

As long as the illumination be divergent and we have a fringe pattern reference, the mathematical model doesn't change and the proposed system would work well. Fringes may be vertical parallel, as shown in the performed experiments. They could also be horizontal parallel, and circular [58].

In this work, a parallel vertical fringe pattern was chosen in order to allow a better comparison with the standard fringe projection technique.

The setup used to verify the principle in which our method is based was a DELL multimedia projector with a resolution of 1200x800, a Pixelink CCD camera with maximum resolution of 2048x1536, a beam splitter 70:30 and a screen (the reference plane). The setup is presented in Fig. 4.4. Distance $L_0 + L_1$ was 85.50 *cm*. The

camera and the projector must be carefully aligned to achieve the on-axis projection and viewing. Distance $L_0 + L_1$ is measured from the CCD camera to the beam splitter and from the beam splitter to the reference plane. To calibrate the system camera-projector we have to estimate the parameters L_0 and L_1 from the camera to the reference plane. In order to do that, we projected a set of squares over the reference plane and measured their projected sides in centimeters. Then, we related them with their image sizes in pixels, according to the relationship between the 3D camera and the 2D image coordinates based on a pinhole camera model, whose equation is given by $\frac{p_0}{L_0} = \frac{p_1}{L_1}$ where p_0 is the period distance of the fringe pattern in the reference plane and p_1 is the period distance of the fringe pattern mapped in the camera CCD (image plane) [30]. In this way, we found that $L_0 = 80.63$ *cm* and $L_1 = 4.87$ *cm*. Just like in the standard fringe projection technique, the distance L_0 and L_1 changes between sets of images with the same parameters. The L_0 values reported are then the average of many measurements performed without changing the system parameters. The maximum variation of the distance L_0 calculated in this way was 0.67% with respect to the average value for the reported experiment.

The first test we performed was to capture an image of the reference plane, to move the plane 1 *cm* to the front of the reference and to capture the image of the plane when $h(x, y) = 1$ *cm*. The phase difference was calculated and $h(x, y)$ was recovered by using Eq. 4.12. In Fig. 4.5 the phase difference and the calculated $h(x, y)$ are shown. Note that this phase difference is not wrapped. We can see in Fig. 4.5b that the plane recovered is in $h(x, y) = 1$ *cm* but in $x = 0$ the values are indeterminate because when x = 0, $\triangle\phi(x, y) = 0$ and there is an indetermination in the equation Eq. 4.12.

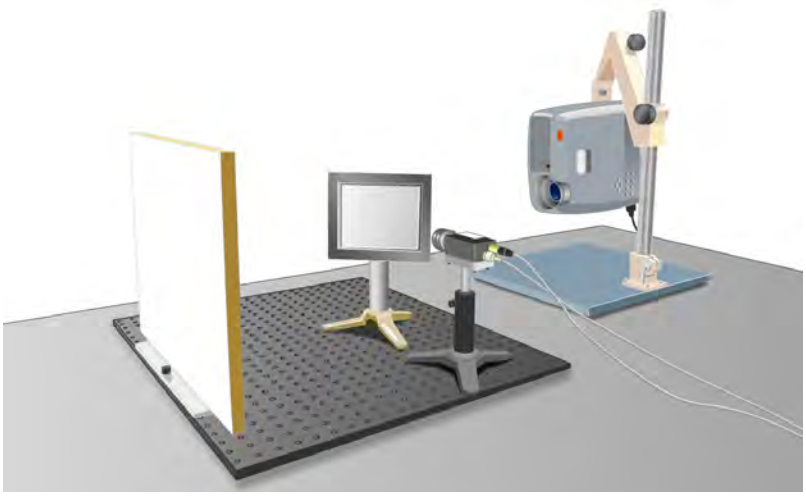

Figure 4.4: Experimental setup that consists of a reference plane, a CCD camera, a projector and a beam splitter 70:30.

After this, we used a test object to compare this method with the standard fringe

projection and the CMM method that we used as a reference. The object was a portion of a sphere with a 4.7 *cm* diameter and 1.2 *cm* tall. A fringe pattern was projected on the screen (the reference plane) with the projector. Two images were recorded by the CCD, the first corresponds to the projected fringes over a reference plane, and the second one corresponds to the projected fringes over the target, as shown in Fig. 4.6.

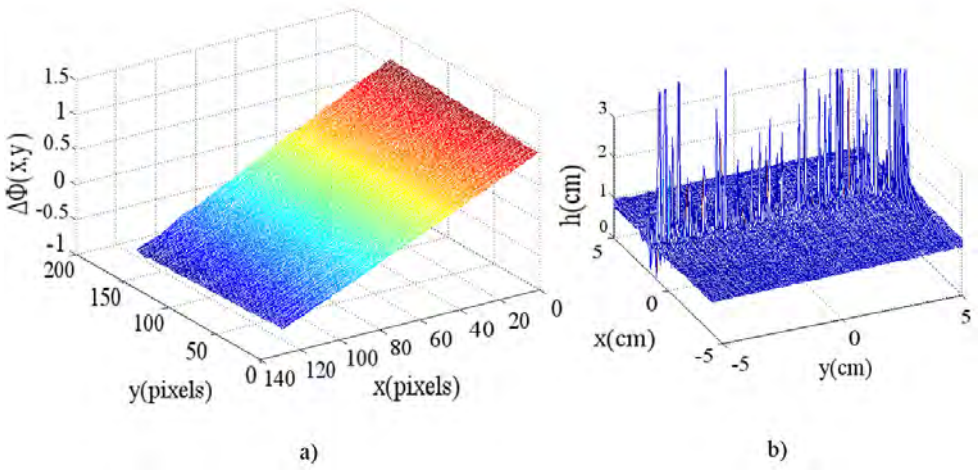

Figure 4.5: Calculation of the phase diference $\Delta\phi(x, y)$ and *h(x, y)*; a) $\Delta\phi(x, y)$ when we move the plane 1 *cm* to the front of the reference, b) height profile, *h(x; y)*, of the plane moved, showing the indeterminated zone.

From Fig. 4.6 we can appreciate that the fringe pattern on the reference plane and over the object is not deformed, but fringes were displaced slightly over the test object. The processing of these images by the proposed method give us the topography information. These images cannot be used to get the topography by using the conventional projected fringes technique. To recover the shape, a 6-step phase shifting method in both images was applied [59]. Afterwards, the phase of both images was obtained, and finally both phases were subtracted and wrapped and *h(x; y)* was obtained. In Fig. 4.7 the phase difference of the test object is shown. We can see that the object was placed out of the optical axis to avoid an indetermination in the Eq. 4.12.

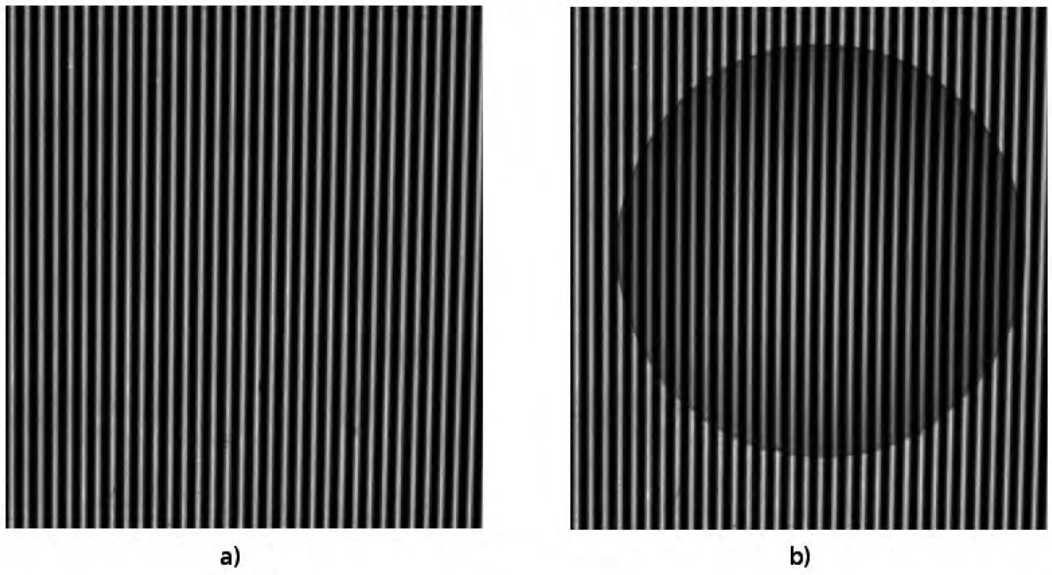

Figure 4.6: Projected fringe pattern : a) reference, b) with the test object.

In Fig. 4.8 the shape of the test object is shown. The topography of the same object by projected fringes, using the same devices and a 6-step phase shifting method can be observed in Fig. 4.9. Both profiles were centered in a new coordinate system x-y for comparison purposes.

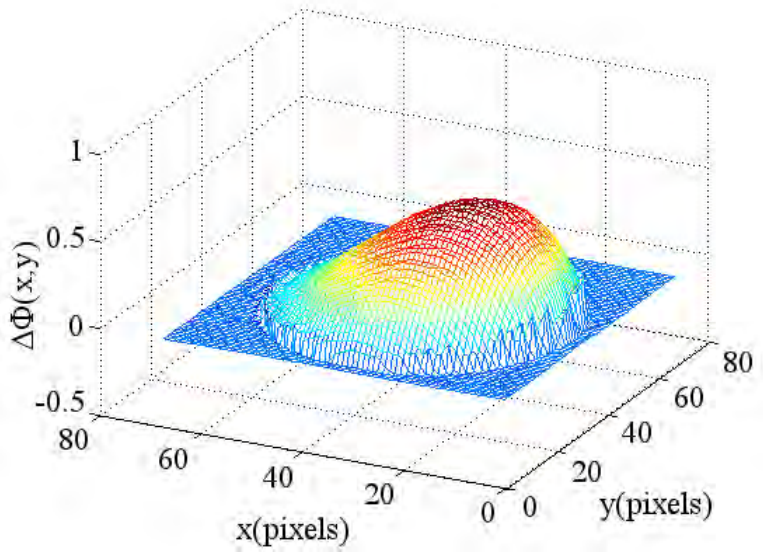

Figure 4.7: Phase difference of the test object.

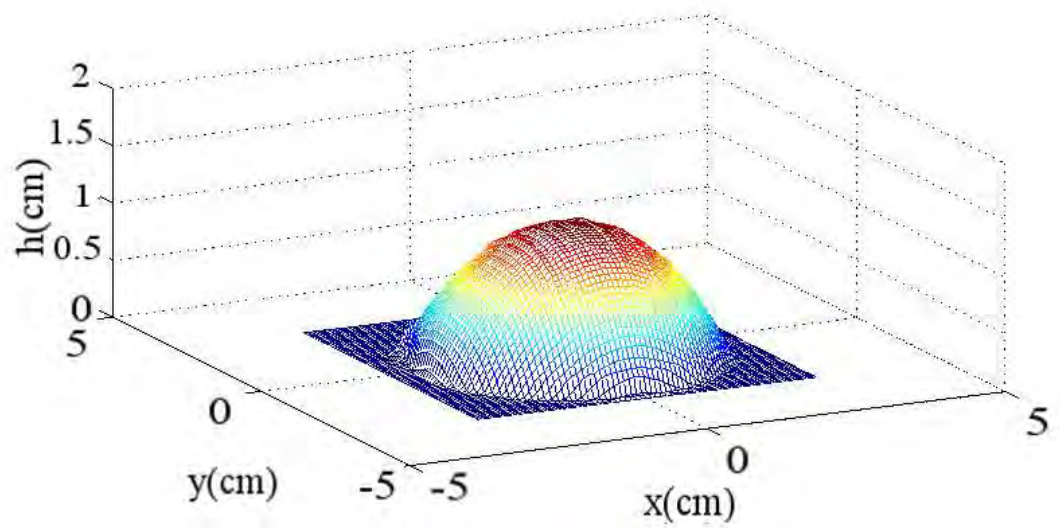

Figure 4.8: Shape of the test object recovered with our proposed method (on axis).

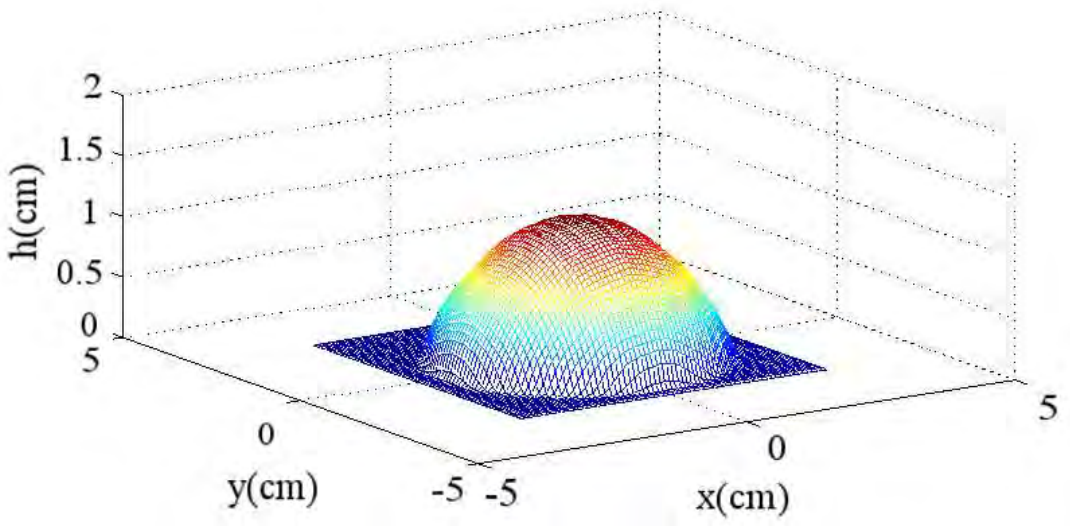

Figure 4.9: Shape of the test object recovered with standard fringe projection (off axis).

It is also possible to obtain the phase of the test object using the Fourier transform method. Although fourier transforms in the two images are very similar are not equal and that difference it allows us to recover the shape of object with good accurately. In Fig. 4.10 the shape of the test object retrieved using the proposed method (on axis

fringe projection) can be observed. If the Fourier transform method is used to calculate the phase of the test object, we must follow the same standard procedure (explained in chapter 5) but without moving the lobe towards the origin of the coordinate system.

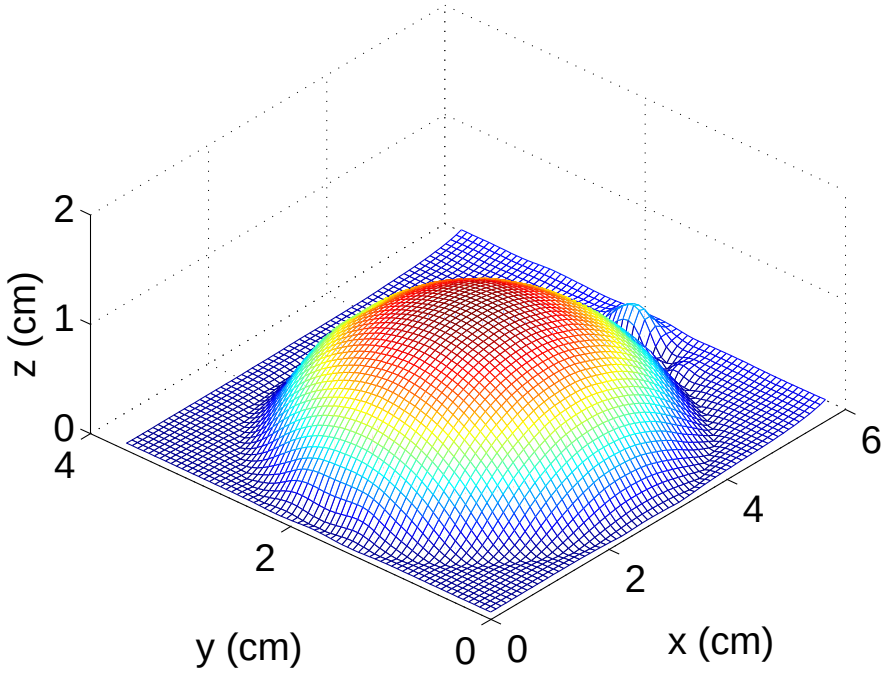

Figure 4.10: Shape of the test object recovered with on axis fringe projection using Fourier transform method to recover the phase.

The signal to noise ratio in the Fig. 4.7 was approximately 16.5 dB. The signal was 45 times biger than the noise. That is, the signal to noise ratio in dB was $10log_{10}(45) = 16.53\ dB$. The signal to noise ratio in Fig. 4.8 was 15.80 dB. The signal to noise ratio obtained by using on axis fringe projection technique and the phase stepping method with 6 steps, was in the same order of the signal to noise ratio obtained when the test object was recover by using standard fringe projection technique and the phase stepping method with 6 step. The phase recovered shown in Fig. 4.9 was obtained using the standard fringe projection method and the phase stepping technique using 6 steps.

4.3.1 Analysis of the results

To analyse the results we compared the profile obtained by using on axis fringe projection and the profile obtained with the standard fringe projection with the one obtained

from a CMM. Fig. 4.11 shows a plane of the topography profiles by using on axis fringe projection, standard fringe projection and the profile obtained with the CMM in a) $y = 0$ and b) $x = 0$. A root-mean-square error (rms) associated to the topography measurement was calculated with the equation [60]:

$$RMS = \sqrt{\frac{1}{N}\sum_{i=1}^{N}\left(h(i) - \hat{h}(i)\right)^2}, \tag{4.13}$$

where $h(i)$ was the result obtained using standard fringe projection and using on axis fringe projection, and $\hat{h}(i)$ was the profile of the CMM that we used as a reference in both cases. The percentage with respect to the maximum height of the object was calculated. The results are shown in Tab. 4.1.

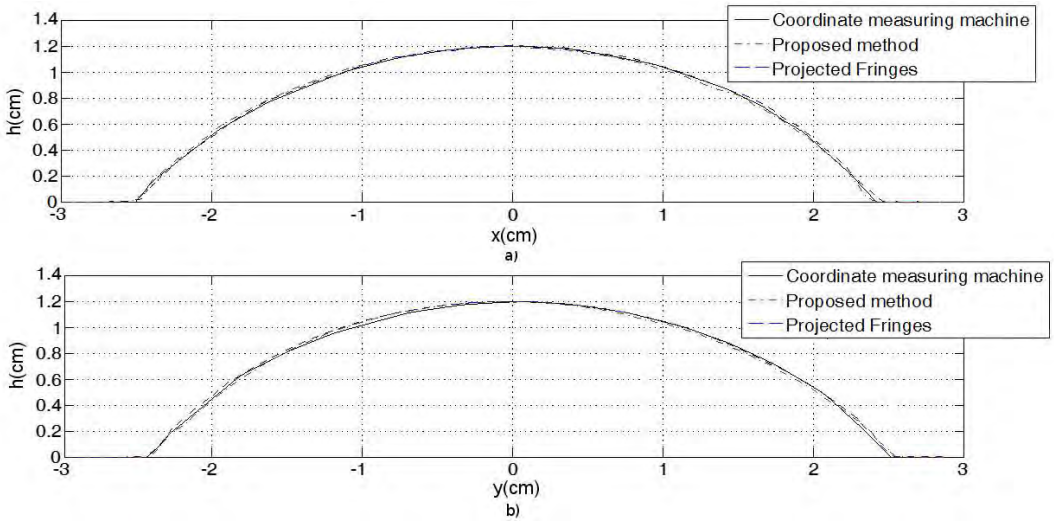

Figure 4.11: Measurements obtained from the CMM (continuos line), fringe projection on axis (dashed-point line) and standard fring projection (dashed line), in: a) $y = 0$, and b) $x = 0$.

	Standard Fringe Projection	On axis Fringe Projection
RMS (%)	1.02	1.16

Table 4.1: Measurement of the root-mean-square error (rms) associated to the topography of the object using the profile of the CMM as a reference.

Fig. 4.13a shows the projected fringes in oblique incidence. In this case, a section of one of the objects (the ramp) is shaded and then it is not possible to evaluate

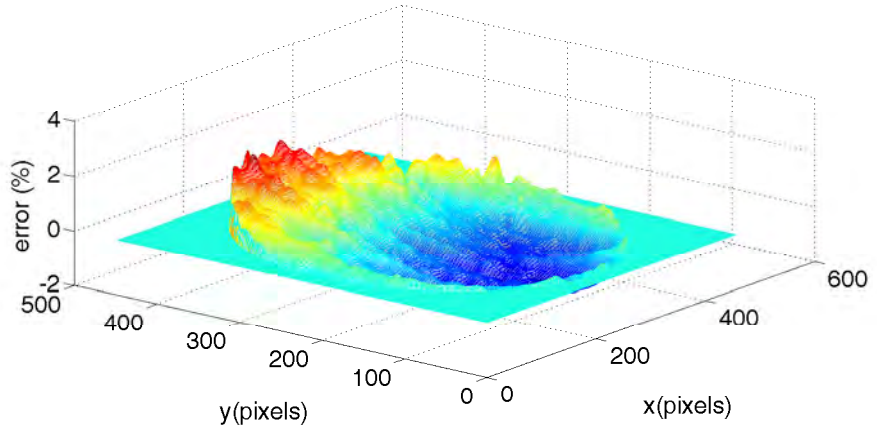

Figure 4.12: Measurement of the error (%): difference between standard fringe projection technique (off axis) and on axis fringe projection technique.

the topography completely. Fig. 4.13b shows the case for projection on axis. The shadow problem is eliminated and the topography can be evaluated for the whole object. In addition, due to the fact that we don't unwrap the phase because all the information is in the range between $(-\pi, \pi)$ we don't have a problem to recover the shape of multiple objects with different heights or objects with surface discontinuities in height [61,62]. Fig. 4.14 shows the automatic recovering of the three different objects without additional processing.

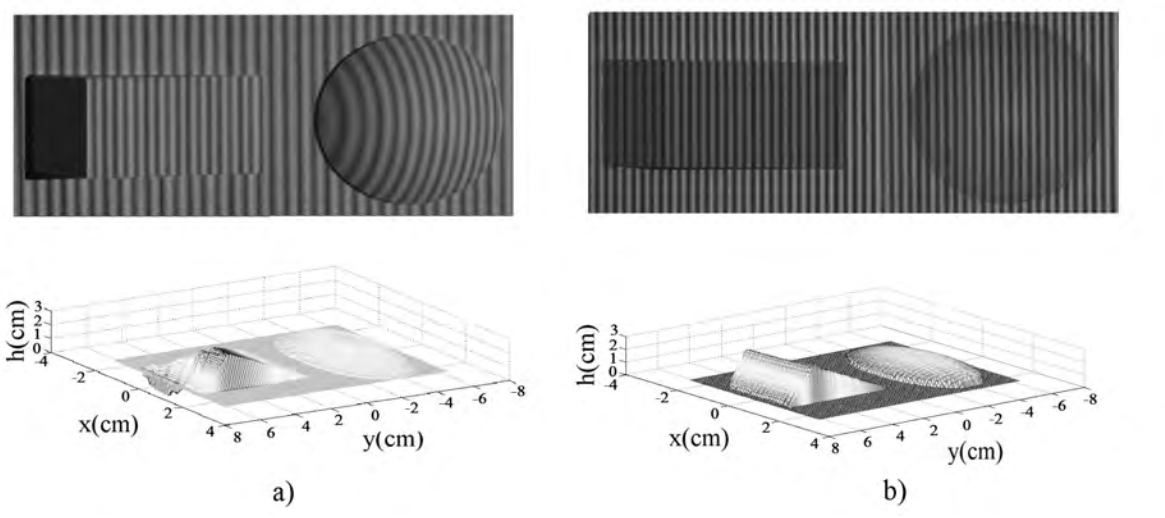

Figure 4.13: Test objects recovered with: a) the projected fringes technique, b) the proposed method.

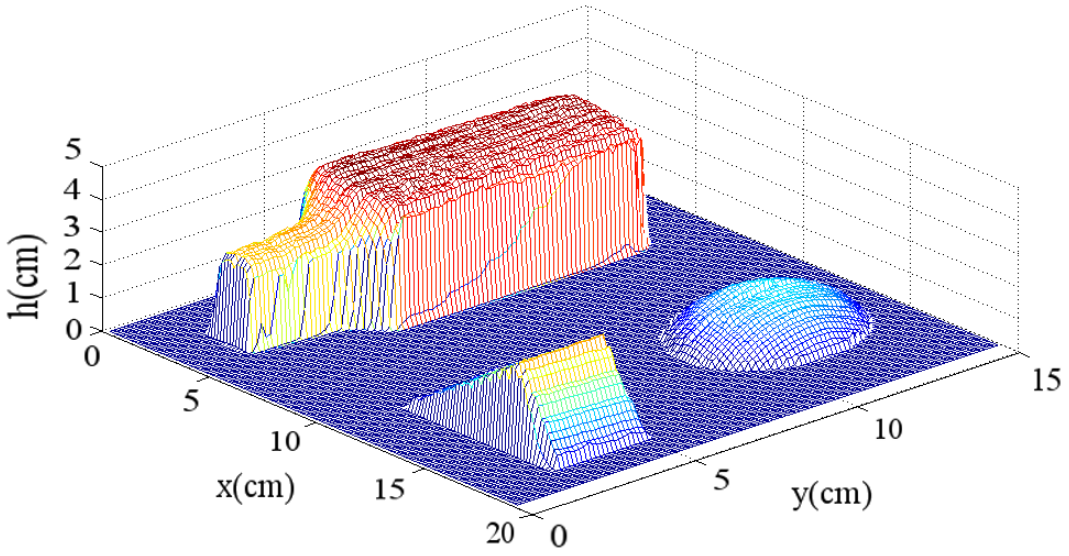

Figure 4.14: Topography of three objects in one shot by projected fringes on axis.

In the Fig. 4.15 shows the phase difference obtained by applying on axis fringe projection of a test object consisting of a theater mask. And in the Fig. 4.16 shows the theater mask recovered using our proposed method. The errors observed in one edge of the recovered mask in Fig. 4.16 are due to the object was very close to the area where information can not be recovered.

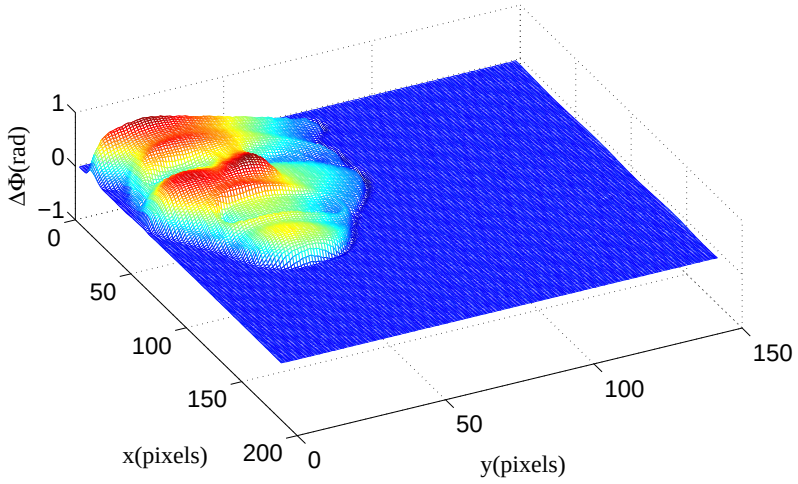

Figure 4.15: Phase difference of a theater mask.

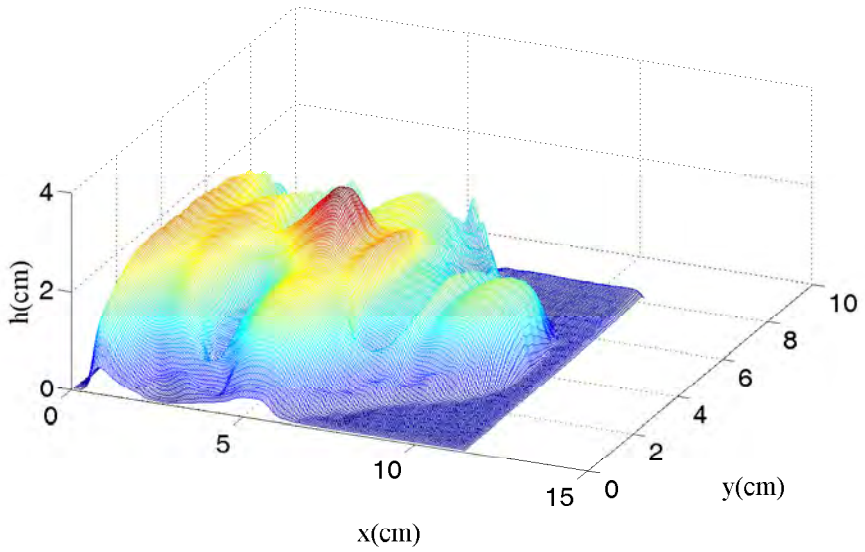

Figure 4.16: Topography of a theater mask.

4.4 Conclusion

In this chapter, we have presented a theoretical analysis supported by experimental results of a new method based on an on axis fringe projection setup. The theoretical analysis used in standard fringe projection systems (off axis) does not work in this setup. The results, using this new method, are in good agreement with those obtained with standard fringe projection and a coordinate measuring machine. The new method has the advantage that the problem of shading is reduced considerably due to the fact that the projected fringes and the observation position are on axis. In this setup, the phase differences are very small, so for many of the objects to be measured, the phase difference is in the range $(-\pi, \pi)$, therefore, the phase difference is not wrapped and we do not need a phase unwrapping processing in the *h(x, y)* estimation, avoiding problems like the 2π phase ambiguity due to measurements of surfaces with height discontinuities greater than the period of the fringe pattern. The system only needs simple calibration to obtain good results. Even though the topography information at $x = 0$ is lost, it can be obtained by interpolation or, alternatively, the object can be placed at a position different than the optical axis and its topography can be then completely evaluated.

In this new method, phase differences are small compared with those calculated in the standard fringe projection technique under the same conditions. Therefore, they have a smaller signal-to-noise ratio and indeed this technique is more sensitive to the noise produced by the camera sensor. However, by using 6-steps in the phase shifting

method to recover the phase, a signal-to-noise-ratio comparable to the standard fringe projection technique can be obtained, as can be seen in our experimental results.

5 Phase recovery algorithms

This chapter briefly describes the phase retrieval algorithms that were used in the works reported in this dissertation: the Phase stepping technique and the Fourier transform technique.

5.1 Phase stepping technique

The techniques used for determining phase are divided into two classes: electronic techniques and analytical techniques. *Analytical techniques:* While the phase is modulated temporarily, information intensity data is stored in a computer and used to calculate the relative intensity measurements. *Electronic techniques:* This technique is widely used to measure distances using interferometers and where necessary to know the phase of a single point with a quick update. To uses this method to measure areas instead of distances, it is necessary to scan the whole surface with a sensor, or to have many sensors attached to the system. Electronic techniques are also called *heterodyne interferometry* [59].

Analytical methods, in turn, can be classified into the following two groups: *1) Integrating bucket phase shifting*: This technique is based on integrating the intensity of the signal as the phase increase linearly. *2) Phase Stepping or Phase Shifting*: This technique is widely used to recover the phase, and as it is one of the techniques used in the works reported in this dissertation, it will be explained next [59].

The general expression for an interference pattern is given by :

$$I = a + b\cos\left(\psi + \alpha\right) \ , \tag{5.1}$$

where a is the background noise, b is the modulation noise, and ψ is the phase difference of the interference pattern. Eq. 5.1 has three unknowns and to completely solve it a system of three equations is needed. [59]

$$\begin{cases} I_1 = & a + b\cos\left(\psi + \alpha_1\right) \\ I_2 = & a + b\cos\left(\psi + \alpha_2\right) \\ I_3 = & a + b\cos\left(\psi + \alpha_3\right) \end{cases} \ . \tag{5.2}$$

If we analyze the system in the interval $(0, \pi)$, and $\alpha_1 = \pi/4$, $\alpha_2 = 3\pi/4$, and $\alpha_3 = 5\pi/4$, ψ can be calculated as: [59]

$$\psi = \tan^{-1}\left[\frac{I_2 - I_3}{I_2 - I_1}\right] . \tag{5.3}$$

However, it is better to use more equations to obtain an overdetermined system, thus having more points of measurement to avoid numerical instabilities. The number of steps that is used most frequently is *4* with an interval of $\pi/2$ [59].

In general, for the kth stepped phase, the resulting intensity can be written as:

$$\psi = \tan^{-1}\left[\frac{\sum_k^N I_k \sin\left(\frac{2\pi k}{N}\right)}{\sum_k^N I_k \cos\left(\frac{2\pi k}{N}\right)}\right] , \tag{5.4}$$

with a shift of $2\pi/N$ per exposure. In Fig. 5.1, a fringe pattern with four steps is shown.

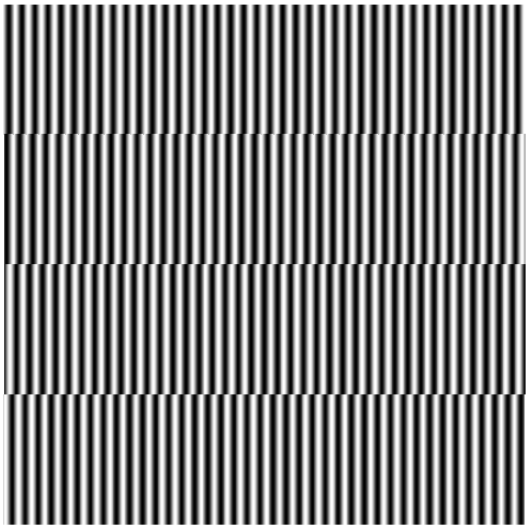

Figure 5.1: Fringe pattern with a four step phase shift $(0, \pi/2, \pi, 3\pi/2)$.

5.2 Fourier transform technique

As seen in the previous section, the expression for an interference pattern is given by:

$$i(x,y) = a(x,y) + b(x,y)\cos\left(2\pi f_0 x + \psi(x,y)\right) \ , \tag{5.5}$$

where a and b represent non-uniform lighting environment (due to reflection, transmission, etc.), $\psi(x,y)$ is the phase difference containing the information we want to obtain, and f_0 is the spatial carrier frequency [14].

Now, we define *c(x, y)* as

$$c(x,y) = \frac{1}{2} b(x,\, y) e^{j\psi(x,\,y)} \ , \tag{5.6}$$

where j is the imaginary unit (defined by $j^2 = -1$). Now, if we write Eq. 5.5 in complex form, the following expression is obtained

$$i(x,y) = a(x,\, y) + c(x,y)e^{2\pi f_0 x} + c^*(x,\, y)e^{-2\pi f_0 x} \ , \tag{5.7}$$

being *c*(x, y)* the complex conjugate of *c(x, y)*.

The Fourier transform of Eq. 5.7 in the x direction is given by

$$I(f,\, y) = A(f,\, y) + C(f - f_0,\, y) + C^*(f - f_0,\, y) \ , \tag{5.8}$$

where A , C and C * are Fourier transforms of a, c, and c *, respectively [14].

Since the spatial variations of $a(x,y)$, $b(x,y)$, and $\psi(x,y)$ are slow compared with the spatial frequency f, the Fourier spectra in Eq. 5.8 are separated by the carrier frequency f, as is shown schematically in figure Fig. 5.2a. We make use of either of the two spectra on the carrier, say $C(f - f_0, y)$, and translate it by f_0 on the frequency axis toward the origin to obtain $C(f,y)$, as is shown in figure Fig. 5.2b. Note that the unwanted background variation $a(x,y)$ has been filtered out in this stage. Again, by using the FFT algorithm, we compute the inverse Fourier transform of $C(f,y)$ with respect to f and obtain $c(x,y)$, defined by Eq. 5.6.

Fig. 5.2a shows a diagram of the power spectrum of the Eq. 5.8. Because a and *c(b,*ψ*)* are functions that vary slowly compared to the carrier frequency f_0, a separation of

the Fourier spectra is observed. Now only one lobe of the spectrum should be used, for example $C\,(f - f_0,\, y)$, and it should be moved towards the origin of the coordinate system a distance f_0, as shown in Fig. 5.2b. Finally calculating the inverse Fourier transform $C\,(f - f_0,\, y)$ with respect to f, $c(x,\ y)$ is again obtained and the phase $\psi(x,\, y)$ can be calculated using the following equation:

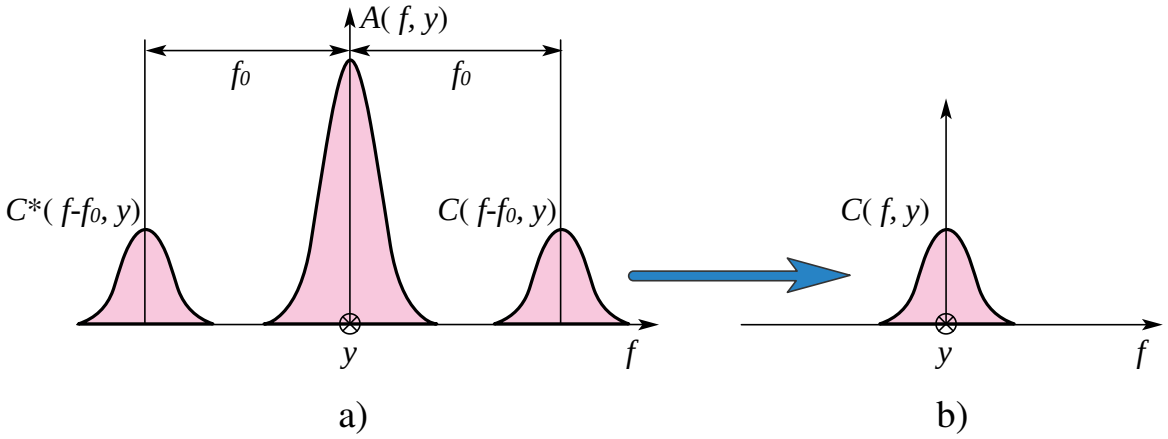

Figure 5.2: a) Diagram of the power spectrum; b) Single lobe of the spectrum selected and translated to the origin. The y axis is normal to the figure.

$$\psi(x,\, y) = \arctan \frac{\mathrm{Im}(c(x,\, y))}{\mathrm{Re}(c(x,\, y))}\,, \tag{5.9}$$

where $\mathrm{Im}\,(c(x,\, y))$ and $\mathrm{Re}\,(c(x,\, y))$ are the imaginary and real part of $c(x,\, y)$, respectively. It is important to remember that the phase obtained is in the range $(-\pi,\, \pi)$ and therefore is indeterminated by a factor of 2π [14].

6 General conclusions and future work

In this thesis, two contributions are made based on the fringe projection technique. In one of them, an interferometric fringe projection using a lateral cyclic shear interferometer is shown, and a study of how the visibility of the fringes affects the reconstruction of the object along the z axis is described. Due to the fact that the cyclic path in this interferometer is quite stable, this optical setup generates stable fringes in poor vibration isolation conditions. Another advantage is that the fringe pattern generated is completely sinusoidal, unlike the one generated with a multimedia projector. Finally, synchronization with a CCD camera is not necessary.

One of the disadvantages of this optical system is that the size of the object to be measured is limited by the size of the beam-splitter, which imposes a limit on the expansion of the beam to cover a large object placed at a short distance.

Problems with speckle generate change in the visibility at large distances, so it is necessary to incorporate a telephoto lens to the CCD camera when the object is large, because the object has to be at a great distance.

The reported method presents speckle noise generated in the measurement of the shape of the test object; however, the noise may decrease if a robust algorithm is used, as it was done in this work.

Finally, in this first work, we also present an analysis of how the visibility of projected fringes affects the evaluation of the topography of an object by means of using fringes generated through interferometry.

In the second work, we have presented a theoretical analysis supported by experimental results from a new method based on an on axis fringe projection setup. The theoretical analysis used in standard fringe projection systems (off axis) does not work in this setup. Using this new method, the results are in good agreement with those obtained with standard fringe projection and a coordinate measuring machine. The new method has the advantage that the problem of shading is reduced considerably due to the fact that the projected fringes and the observation position are on axis. In this setup, the phase difference is within the range $(-\pi, \pi)$; therefore, the phase difference is not wrapped, and we do not need phase unwrapping processing in the $h(x, y)$ estimation, avoiding problems like the 2π phase ambiguity due to measurements of surfaces with height discontinuities greater than the period of the fringe pattern. The system only needs simple calibration to obtain good results. Even though the topography information at $x = 0$ is lost, it can be obtained by interpolation or, alternatively,

the object can be placed at a position different than the optical axis (out of the origin ± 10 pixels as seen on the image plane, approximately) and its topography can be then completely evaluated.

In a standard fringe projection system, sensitivity would be significantly reduced significantly for an angle between projection and detection close to zero, and consequently, the phase difference would not wrap, but if the angle is zero, the shape could not be recovered in spite of having a phase difference greater than zero. However, by using the method proposed in this dissertation, it is possible to recover the shape of an object using an on-axis setup as long as illumination be divergent, because the sensitivity of this technique depends on light divergence.

As a projection system with divergent light is used, there will always be a phase difference, and therefore, it will be possible to recover the shape of the object by means of the proposed technique. In this new method, phase differences are small compared to those calculated in the standard fringe projection technique under the same conditions. Therefore, they have a smaller signal-to-noise ratio, and indeed, this technique is more sensitive to the noise produced by the camera sensor. However, by using 6-steps in the phase shifting method to recover the phase, a signal-to-noise-ratio comparable to the standard fringe projection technique can be obtained, as can be seen in our experimental results. (The signal to noise ratio in the shape recovery of the test object by using the standard fringe projection technique was approximately 17 *dB,* and the signal to noise ratio of the shape recovery of the test object by using the on axis fringe projection technique was approximately 16.5 *dB.*)

For the proposed technique, if the calculated phase difference were greater than 2π, the phase would wrap. This would happen for a height $h(x, y) > L_0 \left({}^{1}/_{1+xf_0}\right)$, toward the edges of the field of view of our camera, if the field were very wide.

As a future work, the shape recovery of technical (engineering) objects will be calculated to apply this method in industry.

The error of topography measurement will be calculated when the same object is placed in different positions over a reference plane by using the projected fringes technique, on and off the optical axis.

A miniaturized version of the on axis fringe projection setup will be developed to measure components within confined volumes.

Published Articles

1. Analía Sicardi-Segade, Amalia Martínez-García, Noel-Ivan Toto-Arellano, J.A. Rayas, "Analysis of the fringes visibility generated by a lateral cyclic shear interferometer in the retrieval of the three-dimensional surface information of an object", *Optik*, Vol 125(3), pp 1320–1324, (2014).
2. Analía Sicardi-Segade, J.C. Estrada, Amalia Martínez-García, Guillermo Garnica, "On axis fringe projection: A new method for shape measurement", *Optics and Lasers in Engineering*, Vol 69, pp 29–34, (2015).

Bibliography

[1] R. S. Sirohi and F. S. Chau, *Optical Methods of Measurement whole field techniques*. Brian J. Thompson, 1999.

[2] J. A. M. Rodriguez, *Recent advances in optical metrology*. J. Apolinar Muñoz Rodriguez, 2007.

[3] P. K. Rastogi, *Optical Measurement Techniques and Aplications*. Artech House, Inc., 1997.

[4] S. S. Gorthi and P. Rastogi, "Fringe projection techniques: Whither we are?," *Opt Laser Eng*, vol. 48, pp. 133–140, 2010.

[5] F. Chen, G. M. Brown, and M. Song, "Overview of three-dimensional shape measurement using optical methods," *Opt Eng*, vol. 39(1), pp. 10–22, 2000.

[6] A. Martínez, J. A. Rayas, H. J. Puga, and K. Genovese, "Iterative estimation of the topography measurement by fringe- projection method with divergent illumination by considering the pitch variation along the x and z directions," *Opt Laser Eng*, vol. 48, pp. 877–881, 2010.

[7] B. Jähne and H. Haubecker, *Three-Dimensional Imagins Techniques, Chap. 7 in Computer vision and applications. A Guide for Students and Practitioners*. Academic press, 2000.

[8] E. K. and H. G., "Acquisition of 3d data by focus sensing," *Appl Opt*, vol. 27, pp. 4684–4689, 1988.

[9] U. Breitmeier, W. Daum, G. Häusler, G. Heinrich, M. Küchel, G. Mollath, W. Nedeborn, a. R. S. a. M. S. H. Schlemmer, and B. Schulze-Willbrenning, P. Sowa, and R. Steinbichler, *Method for optical shape detection*. German Society for zerstörunsfreie examination, 1995.

[10] K. Engelhardt, "Acquisition of 3d data by focus sensing utilizing the moire effect of ccd cameras," *Appl Opt*, vol. 30, 1991.

[11] U. Breitmeier, "Laser profilometry-mebangle biomedical issues," *Biomedizinische Technik*, vol. 38, pp. 99–104, 1993.

[12] G. Häusler and W. Heckler, "Light sectioning with large depth and high resolution," *Appl Opt*, vol. 27, pp. 5165–5169, 1988.

[13] Wikipedia, "http://en.wikipedia.org/wiki/scheimpflug." Scheimpflug principle, 2015.

[14] M. Takeda, H. Ina, and S. Kobayashi, "Fourier-transform method of fringe-pattern analysis for computer-based topography and interferometry„" *J. Opt*, vol. 72, pp. 156–160, 1982.

[15] O. Kafri and I. Glatt, *The phisics of moiré metrology.* joseph W. Goodman, 1990.

[16] H. G. and R. D., "Parallel 3d-sensing by color coded triangulation," *Appl Opt*, vol. 32, pp. 7164–7169, 1993.

[17] Wikipedia, "http://en.wikipedia.org/wiki/theodolite." Theodolite, 2014.

[18] R. Zhang, P.-S. Tsai, J. E. Cryer, and M. Shah, "Shape from shading: A survey," *Faculty of Mathematics and Computer Science*, vol. 21, pp. 690–706, 1999.

[19] R. O'Hara and D. Barnes, "A new shape from shading technique with application to mars express hrsc images," *ISPRS Journal of Photogrammetry and Remote Sensing*, vol. 67, pp. 27–34, 2012.

[20] Y. Z., *Investigation of a 3D-Imaging System based on ORF-Modulation.* PhD thesis, INV,Universität-GH, Siegen, 1998.

[21] U. of Edinburgh, "Holographic interferometry," *Topic 9.*

[22] J. Leendertz, "Interferometric displacement measurement on scattering surfaces utilizing speckle effect," *J. Phys*, vol. 3, pp. 214–218, 1970.

[23] J. N. Butters and J. A. Leendertz, "Speckle pattern and holographic techniques in engineering metrology," *Opt Laser Technol*, vol. 3, pp. 26–30, 1971.

[24] J. C. Dainty, "Laser speckle and related phenomena," *Springer Verlag, Berlin.*, vol. 9, 1975.

[25] R. Jones and C. Wykes, *Holographic and Speckle Interferometry.* Cambridge University Press, Cambridge, 1989.

[26] R. Dändliker and P. Jacquot, "Holographic interferometry and speckle techniques," *Optical Sensors VCH Verlagsgesellschaft, Weinheim*, 1992.

[27] H. K. D. Meinlschmidt, P. and R. S. Sirohi, *Selected Papers on Electronic Speckle Pattern Interferometry: Principles and Practice*, vol. MS 132. SPIE Milestone Series, 1996.

[28] P. Jacquot and J.-M. Fournier, *Interferometry in Speckle Light: Theory and Applications.* Springer, Berlin., 2000.

[29] P. Jacquot, "Speckle interferometry: A review of the principal methods in use for experimental mechanics applications," *The Author. Journal compilation. Blackwell Publishing Ltd Strain*, vol. 44, 2008.

[30] *Shape measurement by speckle interferometry using holographic optical element*, vol. 3744, (Proc. SPIE), 1999.

[31] *Shape measurement using phase shifting speckle interferometry*, vol. 1553, (Proc. SPIE), 1991.

[32] M. Takeda and H. Yamamoto, "Fourier-transform speckle profilometry: three-dimensional shape measurements of diffuse objects with large height steps and/or spatially isolated surfaces," *Appl Opt*, vol. 33, pp. 7829–7837, 1994.

[33] Wikipedia, "http://en.wikipedia.org/wiki/white." White light interferometry, 2014.

[34] D. Tulsiani, *A Fringe Projection System for Measurement of Condensing Fluid Films in Reduced Gravity*. PhD thesis, Worcester Polytechnic Institute, 2005.

[35] K. J. Gasvik, *Moire Methods, Triangulation, Chapter 7 in Optical Metrology*. John Wiley and Sons LDT Third edition, 2002.

[36] *A Simple Laboratory Set-up For The Fringe- Projection Method*, vol. 4588, (Proc. of SPIE), 2002.

[37] *Dynamic moiré patterns and Michelson fringe patterns for profilometry: a results comparative analysis*, vol. 8011, (Proc. of SPIE), 2011.

[38] D. Malacara, *Lateral shearing interferometers, Chap. 4 in Optical Shop Testing*. Second Edition ed Wiley New York, 1992.

[39] P. P. T. Santhanakrishnan and R. S. Sirohi, "Optical configuration in speckle shear interferometry for slope change contouring with a twofold increase in sensitivity," *Appl Opt*, vol. 37, pp. 3447–3449, 1998.

[40] P. K. Rastogi, "An electronic pattern speckle shearing interferometer for the measurement of surface slope variation of three-dimensional objects," *Opt Laser Eng*, vol. 26, pp. 93–100, 1997.

[41] R. K. Tyson, *Wavefront Sensing, Series in optics and optoelectronics, Chap. 5 in Principles of Adaptive Optics*. Third Edition CRC Press Taylor and Francis Group, 2011.

[42] K. Matsuda, Minami, and T. Y. Eiju, "Novel holographic shearing interferometer for measuring lens lateral aberration," *Appl Opt*, vol. 31, pp. 6603–6609, 1992.

[43] D. Ghai, S. Vyas, P. Senthilkumaran, and R. Sirohi, "Detection of phase singularity using a lateral shear interferometer," *Opt Laser Eng*, 2008.

[44] P. K., "Hearing interferometry and the moire method for shear strain determination," *Appl Opt*, 1988.

[45] N. Toto-Arellano, A. Martínez-García, G. Rodríguez-Zurita, J. A. Rayas-Álvarez, and A. Montes-Perez, "Slope measurement of a phase object using a polarizing

phase-shifting high-frequency ronchi grating interferometer," *Appl Opt*, vol. 49, pp. 6402–6408, 2010.

[46] D. I. Serrano-García, N. Toto-Arellano, A. M. García, J. A. R. Álvarez, A. Téllez-Quiñonez, and G. Rodríguez-Zurita, "Simultaneous phase-shifting cyclic interferometer for generation of lateral and radial shear," *Rev Mex Fis*, vol. 57, pp. 255–258, 2011.

[47] N. Toto-Arellano, D. I. Serrano-García, A. M. García, G. R. Zurita, and A. Montes-Pérez, "4d profile of phase objects through the use of a simultaneous phase shifting quasi-common path interferometer," *J. Opt*, vol. 13, pp. 115502–115510, 2011.

[48] J. C. Estrada, M. Servin, and J. A. Quiroga, "Noise robust linear dynamic system for phase unwrapping and smoothing," *Opt Express*, vol. 19, pp. 5126–5133, 2011.

[49] T. Kreis, *Optical Foundations of Holography, Chap. 2 in Holographic interferometry: principles and methods*. Akademie Verlag series optical metrology Akademie Verlag Bremen, 1996.

[50] K. J. Gasvik, "Moire techniques by means of digital image processing," *Appl Opt*, vol. 22, pp. 3543–3548, 1983.

[51] *Wavelet Analysis for Shadow Detection in Fringe Projection Profilometry*, (ISIEA), September 2012.

[52] B. Bringier, A. Bony, and M. Khoudeir, "Specularity and shadow detection for the multisource photometric reconstruction of a textured surface," *J Opt Soc Am A*, vol. 29, pp. 11–21, 2012.

[53] O. A. Skydan, M. J. Lalor, and D. R. Burton, "Technique for phase measurement and surface reconstruction by use of colored structured light," *Appl Opt*, vol. 41, pp. 6104–6117, 2002.

[54] *Shape measurement of objects with large discontinuities and surface isolations using complementary grating projection*, (Proc. SPIE), 1999.

[55] J. Harizanova and V. Sainov, "Three-dimensional profilometry by symmetrical fringes projection technique," *Opt Laser Eng*, vol. 44 (12), pp. 1270–1282, 2006.

[56] M. Sasso, G. Chiappini, G. Palmieri, and D. Amodio, "Superimposed fringe projection for three-dimensional shape acquisition by image analysis," *Appl Opt*, vol. 48 (13), pp. 2410–2420, 2009.

[57] B. Jähne, *From Objects to Images, Chap. 1 in Practical handbook on Image processing for scientific application*. La Jolla, California., 1997.

[58] M. Servín, "Synchronous phase-demodulation of concentric-rings placido mires in corneal topography and wavefront aberrometry (theoetical considerations)," *Cornell University Library http://arxiv.org/abs/1203.1886v2*, 2012.

[59] K. J. Gasvik, *Fringe Analysis, Chap. 11 in Optical Metrology.* John Wiley and Sons LDT Third edition, 2002.

[60] W. J. Dixon and J. F. J. Massey, *Introduccion to measures of central value and dispersion, Chap. 3 in Introduction to statistical analysis.* International student edition, McGraw-Hill Kogakusha, 1969.

[61] Y. Huddart, J. Valera, N.J.Weston, and A. Moore, "Absolute phase measurement in fringe projection using multiple perspectives," *Opt Express*, vol. 21(18), pp. 21119–21130, 2013.

[62] Z. Wang, H. Du, and H. Bi, "Out-of-plane shape determination in generalized fringe projection profilometry," *Opt Express*, vol. 14(25), pp. 12122–12133, 2006.